University of Alberta

Real-Time Updating of a Dynamic Fundamental Model for

Froth Flotation Process

by

Masih Sekhavat

A thesis submitted to the Faculty of Graduate Studies and Research
in partial fulfillment of the requirements for the degree of

Master of Science

in

Process Control

Department of Chemical and Materials Engineering

© Masih Sekhavat
Spring 2014
Edmonton, Alberta

Permission is hereby granted to the University of Alberta Libraries to reproduce single copies of this thesis and to lend or sell such copies for private, scholarly or scientific research purposes only. Where the thesis is converted to, or otherwise made available in digital form, the University of Alberta will advise potential users of the thesis of these terms.

The author reserves all other publication and other rights in association with the copyright in the thesis and, except as herein before provided, neither the thesis nor any substantial portion thereof may be printed or otherwise reproduced in any material form whatsoever without the author's prior written permission.

Abstract

Froth flotation is one of the most common methods in the mineral industry for selective extraction of a small fraction of desired mineral from a finely mixed ground ore.

This work explores the development of a fundamental dynamic model for froth flotation with parameters of the model being estimated and updated online with applicable techniques such as extended Kalman filtering. In the first step, a fundamental dynamic model was proposed and then a series of flotation experiments in a JK Tech batch flotation cell were designed and performed by the Fractional Factorial Design method. In the second step, the developed model was reconciled with dynamic data from the batch flotation cell, and model parameters were estimated and updated on-line using extended Kalman filtering.

Results show the applicability of the Kalman filter estimator for tracking changes in operational conditions and in parameter estimation when disturbances were applied to the system.

Acknowledgement

First, I would like to express the deepest appreciation to my supervisor, Dr. Vinay Prasad and my co-supervisor Dr. Stevan Dubljevic who supported me throughout my thesis with guidance and patience and without that; I would not have completed my master's.

Next, I would like to express my sincere thanks to Dr. Qi Liu and Artin Afacan who led me with great patience with various meetings and being always ready to share their valuable experience and knowledge with me.

Many others have contributed to the accomplishment of this work with me. I also would like to acknowledge the support of my great colleague, Khushaal Popli, who collaborated and helped me in all phases of the project.

Finally, I would like to convey my deepest gratitude to my family, especially my mom, whose encouragement never stopped during my research, my friend Navid for helping me with his advice for writing the thesis and the rest of my friends: Hamidreza, Ardalan, Lili, Beniamin and Marjan, who were great support for me.

Contents

List of figures

List of Tables

Nomenclature

R_f	froth zone recovery (%)
FRT	froth Retention time (s)
k	flotation rate constant (s^{-1})
α	air recovery (%)
Σ	dynamic stability factor (s)
S_b	bubble surface area flux (s^{-1})
J_g	superficial gas velocity (m s^{-1})
v_f	velocity of the top surface of the froth (m s^{-1})
H	Height of froth (m)
V	Total volumetric flow rate of overflowing forth ($m^3 s^{-1}$)
Ψ_b	flow rate of bubble surface area overflowing the weir ($m^2 s^{-1}$)
$\mathcal{E}$	The fraction of air in the overflowing (unitless)
$\overline{S_b}$	average specific surface area (s^{-1})
λ	length of Plateau border (m^{-2})
A_p	cross-sectional area of Plateau borders (m^2)
R	the radius of the bubble sphere (mm)
Γ	total volumetric flow rate of Plateau borders in the overflowing froth ($m^3 s^{-1}$)
Φ_v	volumetric fraction flow rate of valuable material in concentrate ($m^3 s^{-1}$)
Φ_g	volumetric fraction flow rate of gangue in concentrate ($m^3 s^{-1}$)

Φ_w	volumetric fraction flow rate of water in concentrate ($m^3 s^{-1}$)
$\mathcal{E}_w^{pb}$	volumetric fraction of valuable material in the Plateau borders (unitless)
$\mathcal{E}_v^{pb}$	volumetric fraction of water in the Plateau borders (unitless)
$\mathcal{E}_g^{pb}$	volumetric fraction of gangue in the Plateau borders (unitless)
δ_{la}	lamellae thickness (m)
C_w^{la}	concentration of water in the lamellae ($kg\ m^{-3}$)
C_v^{la}	concentration of valuable material in the lamellae ($kg\ m^{-3}$)
A	cross-sectional area of the Plateau border (m^2)
C_{pB}	Plateau border drag coefficient (unitless)
v_g	vertical gas velocity above the lip ($m\ s^{-1}$)
h_{foam}	height of the foam (m)
$h_{overflow}$	height of the overflowing foam (m)
R	overall recovery (%)
τ	mean residence time (s)
FD	froth depth (m)
R_f	froth zone recovery (%)
V_g	superficial velocity of the air ($s^{-1}\ m^{-1}$)
P	probability of collection (unitless)
R_2	single air bubble of radius (m)
D	diameter of flotation column (m)
P_a	probability of adhesion (%)

P_c	probability of bubble-particle collision (%)
P_d	probability of detachment (%)
Ψ	empirical stream function (unitless)
X	radial coordination (unitless)
R	normalized bubble radius (unitless)
r_c	critical radius (m)
E_1	energy barrier (J)
E_2	secondary energy minimum (J)
W_a	work of adhesion (J)
V	sum of three interaction energies (J)
V_e	electrostatic energy (J)
V_d	dispersion energy (J)
V_h	hydrophobic energy (J)
Φ_1	stern potentials of the bubble (J)
Φ_2	stern potentials of the particle (J)
1/ κ	Debye length (m^{-1})
A_{123}	Hamaker constant of particle 1 and bubble 2 interacting in a medium 3 (J)
E_k'	kinetic energy that makes the particles to be detached from the bubble surface (J)
γ_{lv}	surface free energies at liquid/vapor interfaces (Nm^{-1})
θ	contact angle (∘)
V_p	volume of pulp (m^3)

V_f	volume of froth (m^3)
x_b	concentration of particles on the surface of the bubbles in the pulp ($kg\ m^{-3}$)
x_p	concentration of particles free in the pulp ($kg\ m^{-3}$)
x_c	concentration of particles attached in the froth ($kg\ m^{-3}$)
k_1	first order rate constant for attachment (s^{-1})
k_2	first order rate constant for detachment (s^{-1})
Q_{air}	air flow-rate ($m^3 s^{-1}$)
Q_E	volumetric flow-rate of slurry from the pulp to the froth layer ($m^3 s^{-1}$)
$Q_{E'}$	volumetric flow-rate of drainage from the froth layer to the pulp phase ($m^3 s^{-1}$)
Q_c	volumetric flow-rate of product in the concentrate ($m^3 s^{-1}$)
N_p	number of particles ready for the collision (unitless)
N_B	number of bubbles ready for the collision (unitless)
U_t	turbulent aggregate velocity ($m\ s^{-1}$)
n_B^f	concentrations of free bubbles (number of bubbles/m^{-3})
n_p^f	concentrations of free particles (number of particles/m^{-3})
k'	pseudo-rate constant (s^{-1})
Z	bubble-particle collision frequency (s^{-1})
P_c	probability of bubble-particle collision (%)
P_{asl}	probability of bubble-particle attachment by sliding (%)

P_{tpc}	probability of forming a three-phase contact (%)
P_{stab}	probability of bubble-particle aggregate remaining stable (%)
R_p	particle radius (m)
R_B	bubble radius (m)
G	dimensionless particle settling velocity (unitless)
υ_{ps}	particle settling velocity ($m\ s^{-1}$)
υ_B	bubble rise velocity ($m\ s^{-1}$)
μ_l	liquid dynamic viscosity (Pa.s)
ρ_l	liquid density ($kg\ m^{-3}$)
ρ_p	Particle density ($kg\ m^{-3}$)
d_B	the bubble diameter (m)
F	fluid friction factor (unitless)
h_{crit}	liquid film thickness at time that the film starts to ruptures (m)
C_B	constant for representing the bubble surface mobility (unitless)
h_0	initial thickness of the film at the time the sliding process begin (m)
Z'	detachment frequency (s^{-1})

Chapter 1

1 Introduction

1.1 General description

Froth flotation is one of the most common methods in mineral processing for the selective extraction of a small fraction of desired mineral from a finely mixed ground ore based on differences in the hydrophobicity of the mineral and the rest of the ore, and consequently its ability to adhere to the surface of air bubbles. The flotation process consists of several sub-processes in which, at first, the air bubbles are injected into a vessel containing a slurry with a finely ground mixture of minerals. Particles are kept in suspension in the flotation cell through agitation by an impeller. Those particles that are hydrophobicized attach to the rising bubbles, which leads to the formation of bubble-solid aggregates. The aggregates move up along the cell and reach the froth phase and are finally collected in the concentrate as a valuable product. Those hydrophilic particles that do not attach to the bubbles remain at the bottom of the cell and are collected as non-valuable product (tailing) (Viller et al., 2010). The main goal in the froth flotation process is to maximize grade and recovery of the desired mineral (Fuerstenau, 2007).

Achieving a good understanding of the flotation process requires that all the relevant sub-processes taken into consideration. Many investigations regarding the sub-processes including bubble-particle interactions, transfer of particles from the pulp phase to the froth phase by attaching to the air bubbles, dropback of

particles from froth phase to pulp phase, the conditions of impeller and mixing, solid entrainment and froth stability have been considered in previous studies. Nonetheless, a comprehensive model which could describe the whole process and sub-processes in a general framework has not been developed previously (Cruz, 1997).

There are some mathematical models that could describe the transferr of hydrophobic particles from the pulp phase to the froth phase and finally to the concentrate. These models are examined in different operating conditions such as perfectly mixed or plug flow (Dobby and Finch, 1986a; Luttrel and Yoon, 1991). In most of these models, a first-order rate process is considered as a main key in representing the flotation of particles. Relating the recovery of the mineral species to characteristic factors such as air flow-rate, bubble and particle sizes, slurry residence time and impeller speed in the pulp zone is regarded as a main challenge in mathematical models (Cruz, 1997).

1.2 Objectives

The primary objective of this present investigation is to develop a fundamental dynamic model for froth flotation with parameters of the model being estimated and updated continuously on-line in real time based on comparison of the model predictions with experimental data.

The stage-wise objectives of this research are:

1. Analyzing and investigating various models for froth flotation
2. Categorizing models based on different levels of complexity

3. Proposing and developing a dynamic fundamental model for flotation processes
4. Structuring the state-space form of the proposed model
5. Designing and performing a series of flotation experiments under different operating conditions
6. Fitting the model to the experimental data
7. Performing offline parameter estimation
8. Performing online parameter estimation using Kalman filter
9. Real-time updating of model parameters
10. Predicting the recovery of the system
11. Comparing the experimental recovery with the predicted recovery

1.3 Thesis outline

In the current research, a fundamental model for froth flotation processes is developed. In chapter 2, a review of the literature and background related to the topics in this research, including the specifics of froth flotation processes, flotation models based on foam physics, two-phase flotation models, three-phase flotation models, kinetics of froth transportation, froth zone recovery models, application of DLVO theory for determining flotation rate constants, and models based on micro-process probabilities are discussed. Chapter 3 contains the experimental design, materials and methods. Chapter 4 discusses the proposed model and real-time parameter estimation in different scenarios with and without

disturbances in operating conditions. Chapter 5 contains the summary of this research and also suggestions for future work.

Chapter 2

2 Background and literature review on flotation modeling

2.1 General definitions and structures in flotation process

A flotation cell consists of two distinct phases, a pulp phase and a froth phase. The pulp phase has been taken into consideration extensively in previous studies. It has been determined recently that the froth phase is a significant part of the process and has a major effect on the final performance of flotation process (Vera et al., 2002). In order to investigate the modeling of floatation process properly, there should be an initial introduction to the main factors and performance measures that are involved in the process. These are:

1. Froth zone recovery (R_f), defined as the recovery by only true flotation (particles entering the froth zone to from the collection zone by attaching to the bubbles) (Vera et al., 2002)
2. Froth retention time (FRT), defined as the ratio of froth volume to the volumetric flow-rate of concentrate form the flotation cell (Vera et al., 2002)
3. Flotation rate constant (k)
4. Air recovery (α), defined as the ratio of unbroken bubbles overflowing from the cell to the amount of air introduced in the flotation cell (Vera et al., 2002)

5. Dynamic stability factor (Σ), defined as the ratio of the total volume of the froth at equilibrium to the injected volumetric air flow-rate to the flotation cell (Bikerman, 1973)
6. Air hold-up, defined as the ratio of volumetric fraction of air to the overall volumetric fraction of air and pulp
7. Bubble surface area flux (S_b), defined as the total surface area of rising bubbles in a flotation cell through a unit cell cross sectional area per unit time (Finch et al.,1990)
8. Superficial gas velocity (J_g)

2.2 Modelling the flotation process based on the foam physics

Due to the complex nature of foams, foams have been of interest to mathematicians and physicists for a long time. Pioneering work on foams was done by J. A. F. Plateau in 1873. Much research on various aspects of foams has been performed to realise the structure of the foams. It has been recognized that foam films at stable equilibrium can only meet along lines called Plateau borders, with an angle of 120° between them. Moreover, four of these Plateau borders with an angle of 109° between them, must meet in order to form a vertex. A two-phase foam consists of gas cells that are surrounded by liquid. In a typical foam, the bubbles are in the form of polyhedral cells with their surfaces covered by thin films (lamellae). The thin films meet in Plateau borders and the Plateau borders meet at vertices (Bikerman, 1973; Weaire and Hutzler, 1999). In other words, as is shown in figure 2.1, lamellae refer to the thin water films that separates the

bubbles, and at the intersection of three lamellae, a channel called a Plateau border is formed.

Ventura-Medina and Cilliers (2002) developed a model to describe flotation performance based on the physics of foams and froth image analysis. In their proposed model, it is assumed that the total amount of material in the froth phase is either in the lamellae (bubble shell) or in the Plateau borders, as shown in figure 2.2.

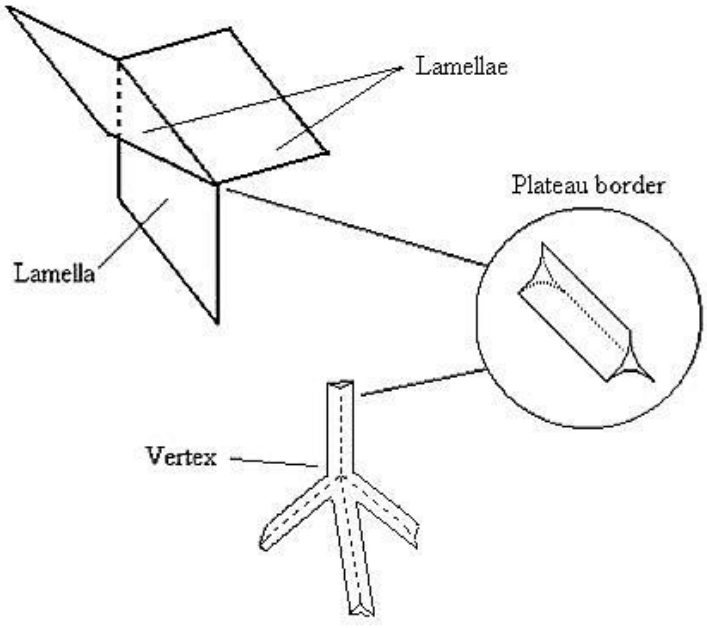

Figure 2-1: Formation of lamellae, Plateau borders and vertices (Ventura-Medins and Cilliers, 2002)

Both lamellae and Plateau border contributions are related to the total volumetric flow rate of overflowing froth:

$$V = v_f hw \tag{2.1}$$

where v_f is the velocity of the top surface of the froth; h is the height of froth overflowing the weir and w is the width of the weir. For the contribution of the lamellae, the amount of material can be calculated by the total surface area of froth overflowing the weir. The flow rate of bubble surface area overflowing the weir is given by

$$\Psi_b = \mathcal{E}\, V\, \overline{S_b} \tag{2.2}$$

where $\mathcal{E}$ is the fraction of air in the overflowing froth and $\overline{S_b}$ is the average specific surface area of the froth, which can be estimated by image processing.

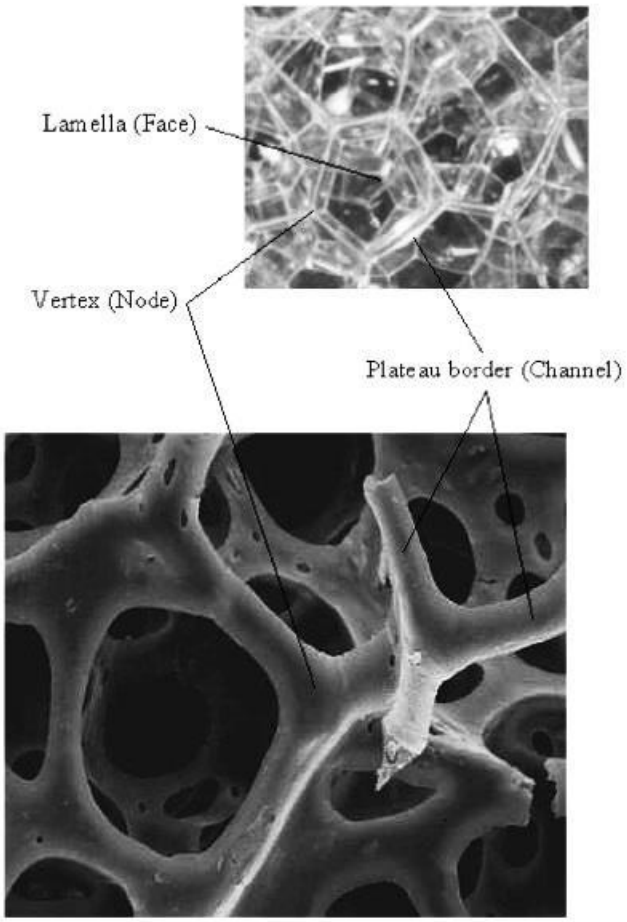

Figure 2-2: Real structure of foams depicting lamellae and Plateau borders (Ventura-Medins and Cilliers, 2002)

For the contribution of the Plateau borders, the volumetric flow rate of Plateau borders in the overflowing froth can be calculated by

$$\frac{\text{Total volume of Plateau borders}}{\text{Total volume of froth}} = \lambda\, A_p \tag{2.3}$$

where A_p represents the cross-sectional area of Plateau borders and λ is the length of Plateau border per unit volume of froth, calculated using

$$\lambda = \frac{1.7037}{R^2} \tag{2.4}$$

where R is the radius of the bubble obtained from the image processing.

The total volumetric flow rate of the Plateau borders in the overflowing froth can be quantified by

$$\Gamma = \lambda\, A_p V \tag{2.5}$$

There are three components in the concentrate: valuable material (v), gangue (g) and water (w). The volumetric fraction flow rate of these materials are calculated using the following formulae:

$$\Phi_v = \Psi_b \delta_{la}\, C_v^{la} + \Gamma\, \mathcal{E}_v^{pb} \tag{2.6}$$

$$\Phi_g = \Gamma\, \rho_g \mathcal{E}_g^{pb} \tag{2.7}$$

$$\Phi_w = \Psi_b \delta_{la}\, C_w^{la} + \Gamma\, \rho_w\, \mathcal{E}_w^{pb} \tag{2.8}$$

$$\mathcal{E}_w^{pb} = 1 - \mathcal{E}_g^{pb} - \mathcal{E}_v^{pb} \tag{2.9}$$

where the superscripts “la” and “pb” refer to lamellae and Plateau borders, respectively. C represents the concentration of components in the lamellae and Plateau borders. δ_{la} is the lamellae thickness and $\delta_{la}\ \mathrm{C_i^{la}}$ represents the amount of solids of component I covered the surfaces of the lamellae. $\mathcal{E}_w^{pb}$, $\mathcal{E}_v^{pb}$ and $\mathcal{E}_g^{pb}$ are the volumetric fractions of water, valuable material and gangue in the Plateau borders, respectively.

The unknown parameters are $\mathcal{E}_w^{pb}$, $\mathcal{E}_v^{pb}$, $\mathcal{E}_g^{pb}$ and Γ, which can be estimated by solving equations 2.6 - 2.9. Φ_v, Φ_w, Φ_g, $\delta_{la}\, C_v^{la}$, $\delta_{la}\, C_w^{la}$ and Ψ_b can be calculated from the experimental measurements and image processing.

2.2.1 Modelling the liquid recovery in the flowing foams

The reason that modelling the liquid recovery is significant is that it is proportional to the amount of undesired material recovered in the concentrate. The first mathematical model for recovery was developed by Leonard and Lemlich, 1965; and Verbist et al., 1996. A schematic diagram of flowing foam is given in figure 2.3.

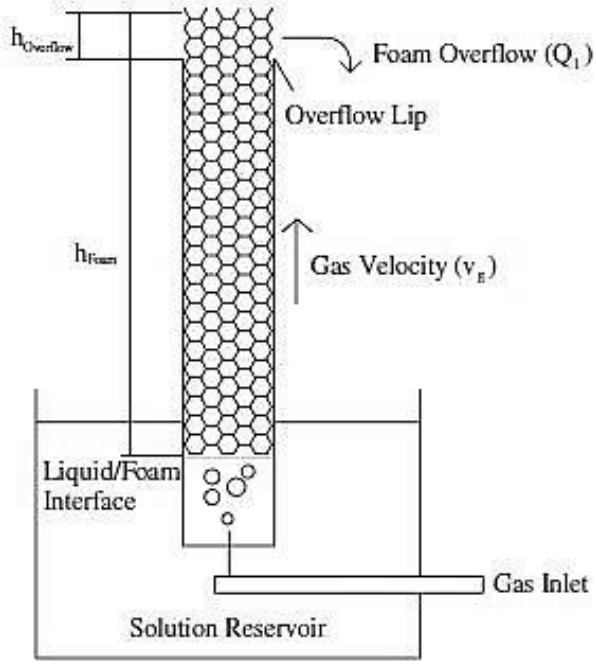

Figure 2-3: Schematic view of a flowing foam (Neethling and Cilliers, 2003)

Assuming that the flow is only in the vertical direction, the following expressions are derived:

$$v_l = -k_1 A - \frac{k_2}{\sqrt{A}} \frac{dA}{dy} + v_g \tag{2.10}$$

where

$$k_1 = \frac{\rho g}{3 C_{pB} \mu} \tag{2.11}$$

$$k_2 = \frac{\left(\sqrt{\sqrt{3} - \frac{\pi}{2}}\right) \gamma}{6 C_{pB} \mu} \tag{2.12}$$

In equations 2.10, 2.11 and 2.12, ρ, γ and μ are the liquid density, surface tension and viscosity, respectively. C_{pB} represents the Plateau border drag coefficient. A is the cross-sectional area of the Plateau border at a given height.

Two sets of equations are considered: (1) below the lip, and (2) over the lip. In the first zone, below the lip, there is no liquid flow rate (removal or addition) except the single liquid flowrate Q_l. Therefore, the following expression is derived:

$$\frac{Q_l}{A_{col}} = \lambda(-k_1 A^2 - k_2 \sqrt{A} \frac{dA}{dy} + v_g A) \tag{2.13}$$

For solving the above problem, a boundary value for A is required:

$$A_{interface} = \frac{\mathcal{E}_{interface}}{\lambda} \tag{2.14}$$

where $\mathcal{E}_{interface}$ is the liquid fraction of the foam at the foam-liquid interface.

The main assumption is that the horizontal liquid flow profile will be the same as the horizontal gas velocity over the lip. Therefore, for the zone above the lip, the following expressions are given:

$$Q_{removal} = \frac{v_{g(out)} l_{lip} A\lambda}{A_{column}} \tag{2.15}$$

$$v_{g(out)} l_{lip} h_{overflow} = v_{g(in)} A_{column} \tag{2.16}$$

Substituting equation 2.16 in equation 2.15 results in

$$Q_{removal} = \frac{v_{g(in)} A\lambda}{h_{overflow}} \tag{2.17}$$

The vertical gas velocity above the lip is given by

$$v_g = v_{g(in)} \frac{h_{foam} - y}{h_{overflow}} \tag{2.18}$$

In equation 2.10, v_g can be substituted by the expression from equation 2.18, leading to

$$v_l = -k_1 A - \frac{k_2}{\sqrt{A}} \frac{dA}{dy} + v_{g(in)} \frac{h_{foam} - y}{h_{overflow}} \tag{2.19}$$

Substituting equations 2.09 and 2.15 into the continuity equation leads to the following expression:

$$\frac{d^2 A}{dy^2} = \frac{-2k_1 A \frac{dA}{dy} - \frac{k_2}{2\sqrt{A}} \left(\frac{dA}{dy}\right)^2 + v_{g(in)} \frac{h_{foam} - y}{h_{overflow}} \frac{dA}{dy}}{k_2 \sqrt{A}} \tag{2.20}$$

Equation 2.20 gives the Plateau border area profile above the lip. The value and the gradient of A in this region are obtained from the solution of equation 2.13. The final boundary condition at the top surface of the foam is given by

$$A_{top} = -\left(\frac{k_2}{k_1}\left(\frac{dA}{dy}\right)_{top}\right)^{\frac{2}{3}} \quad (2.21)$$

2.3 Two Phase Flotation Model

Figure 2.4 represents a schematic diagram of a two-phase flotation model from Vera et al., 1999. As is shown in figure 2.4, there are two zones in flotation processes, the collection zone and the froth zone. The two main assumptions are made by the authors in order to explain the froth zone performance are: (1) the transfer of particles from the pulp zone to the froth zone depends only on the phenomena happening in the pulp zone, and (2) the transfer of particles from the froth zone to the concentrate depends only on the phenomena happening in the froth zone.

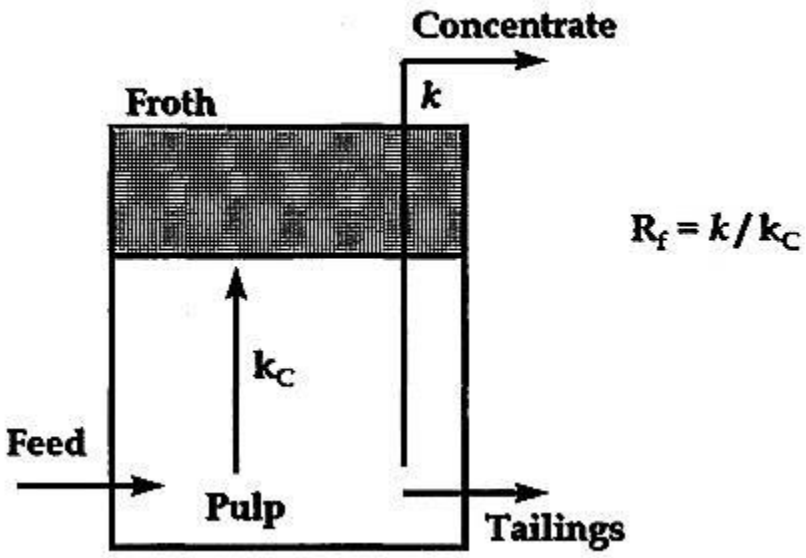

Figure 2-4: Two-phase flotation process (Vera et al., 1999)

The froth zone performance is expressed in terms of the froth zone recovery efficiency which is the total rate of transfer from the pulp zone to concentrate divided by the rate of transfer from pulp zone to the froth zone. Equation 2.10 provides the expression for froth zone recovery:

$$R_f = \frac{k}{k_c} \tag{2.22}$$

where k is the overall flotation rate constant, which can be calculated from the overall recovery by considering the system (all phases together) to be perfectly mixed:

$$k = \frac{R}{\tau(1-R)} \tag{2.23}$$

where R is the overall recovery obtained from experiments and τ is the mean residence time.

In equation 2.22, the flotation rate constant can be related to the froth depth (FD). Several researchers have reported a linear relationship between the flotation rate constant and the FD with a negative slope (Feteris, et al., 1987; Laplante, et al., 1983b; Engelbrecht and Woodburn, 1975). Figure 2.5 depicts the relationship between the flotation rate constant and the FD.

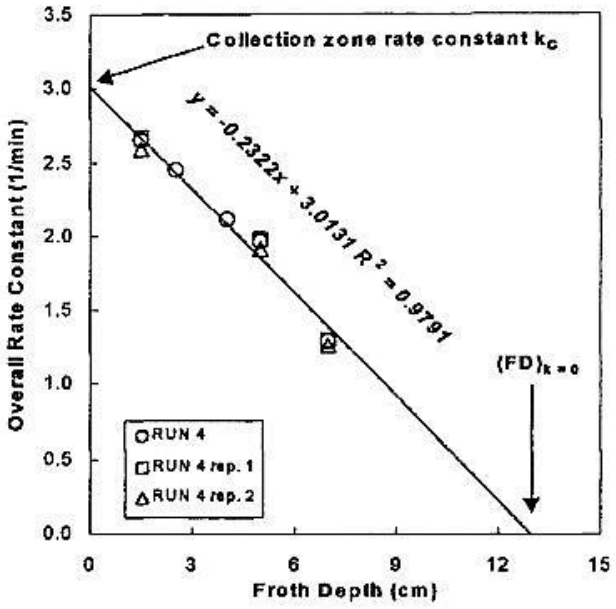

Figure 2-5: Overall rate constant as a function of froth depth (Vera et al., 1999)

Therefore, the relationship can be described as

$$k = a - b(FD) \tag{2.24}$$

When the froth depth is zero, $a = k_c$ will be obtained from the intercept (shown in figure 2.5). Now, by assuming $FD_{k=0}$ to be the intercept of the line with the X-axis when k=0, which means that there is no transfer of material from the froth phase to the concentrate due to a very deep froth, we obtain $b = \frac{k_c}{FD_{k=0}}$ and calculate $k_c = b \times FD_{k=0}$ (Vera et al., 1999). Therefore we have:

$$k = k_c(1 - \frac{FD}{FD_{k=0}}) \tag{2.25}$$

Substituting equation 2.25 in equation 2.22 gives

$$R_f = 1 - \frac{FD}{FD_{k=0}} \tag{2.26}$$

2.4 Three Phase Flotation Model

Figure 2.6 illustrates the structure of the three phase model proposed by Hanumanth and Williams, 1992. Their proposed model consists of a pulp phase and two froth phases and describes the mass transport between these phases by applying various rate constants. In this way, by considering the rise of material through the phases and also the solid drainage in the froth layer, the kinetics of the flotation process can be described. The model is based on the following two assumptions:

1- The pulp phase is perfectly mixed

2- The froth phase is divided into two well-mixed phases. The first phase is exactly above the pulp phase and is called the primary froth layer, and the rest is called the secondary froth layer.

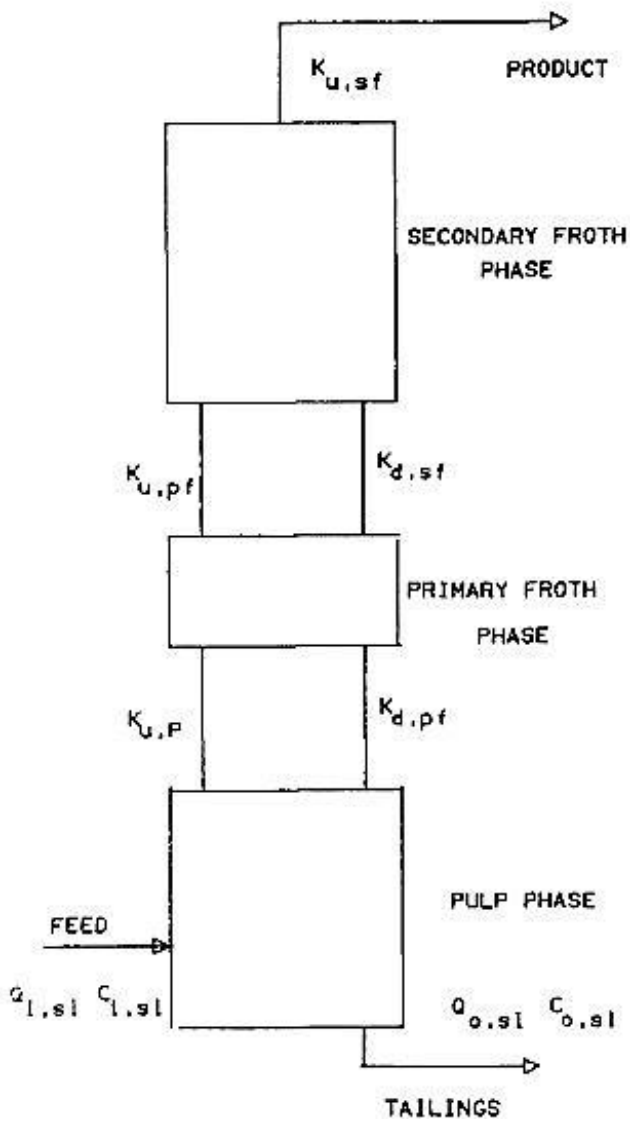

Figure 2-6: Structure of three-phase model (Q, C and K denotes volumetric flowrate, concentration and rate coefficients, respectively) (Hanumanth and Williams, 1992)

Based on these assumptions, the following mass balance is obtained for the pulp phase:

$$\frac{dW_p}{dt} = k_{d,pf}W_{pf} - K_{u,p}W_p - Q_{i,sl}C_{i,sl} - Q_{o,sl}C_{o,sl} \tag{2.27}$$

Knowing that the pulp phase is well-mixed, equation 2.26 can be written as

$$\frac{dW_p}{dt} = k_{d,pf}W_{pf} - aW_p + Q_{i,sl}C_{i,sl} \tag{2.28}$$

where

$$a = K_{u,p} + \frac{Q_{o,sl}}{V_p} \tag{2.29}$$

The mass balance for the primary froth phase is

$$\frac{dW_{pf}}{dt} = K_{u,p}W_{pf} - K_{d,sf}W_{sf} - \left(K_{u,pf} + K_{d,pf}\right)W_{pf} \tag{2.30}$$

and that for the secondary froth phase is

$$\frac{dW_{sf}}{dt} = K_{u,pf}W_{pf} - \left(K_{d,sf} + K_{u,sf}\right)W_{sf} \tag{2.31}$$

In the above equations, the subscripts u, d, sf, pf and p represent upward mass transfer, downward mass transfer, secondary froth phase, primary froth phase and pulp phase, respectively.

Their model provided estimates for the kinetics for pulp phase, froth phase, solid drainage based on experimental measurements of the variation of the froth phase and the recovery.

2.5 Applying the DLVO theory in froth flotation modelling

A flotation model based on hydrodynamic and surface forces was developed by Yoon and Mao, 1996. By using a stream function and estimating the kinetic energies, the hydrodynamic forces were determined and by considering the ion-

electrostatic, London_van der Waals and hydrophobic forces, the surface forces were calculated.

Many researchers have postulated a first order process to describe flotation (Bushell, 1962; Sutherland, 1948). Figure 2.7 shows a single air bubble of radius R_2 rising in an aqueous suspension of particles. By accepting this assumption that the flotation process is a first order process ($\frac{dN}{dt} = -kN$), and that the total number of particles in the suspension is N, the rate of particles that are removed by flotation process is given by

$$\frac{dN}{dt} = -\left(\frac{3}{4}\frac{P}{R_2}V_g\right)N \tag{2.32}$$

where V_g is the superficial velocity of the air, which is defined as the volumetric air flowrate divided by the cross-sectional area of the column, and P is the probability of collection. Therefore, equation 2.32 can be written as

$$k = \frac{3}{4}\frac{V_g}{R_2}P \tag{2.33}$$

where k is the rate constant of the floation process.

Finally, the rate constant can be written as

$$k = \frac{1}{4}S_b P \tag{2.34}$$

where

$$S_b = \frac{3V_g}{R_2} \tag{2.35}$$

S_b is the superficial surface area rate of bubbles, which is defined as the total surface area of rising bubbles in the flotation cell through a unit cell cross sectional area per unit time (Finch et al., 1990). S_b, which is proportional to superficial gas velocity and inversely proportional to the bubble diameter, can be used as a scalable parameter to relate the rate of mineral recovery to physical parameter of the flotation cell (Sawyer et al., 1998).

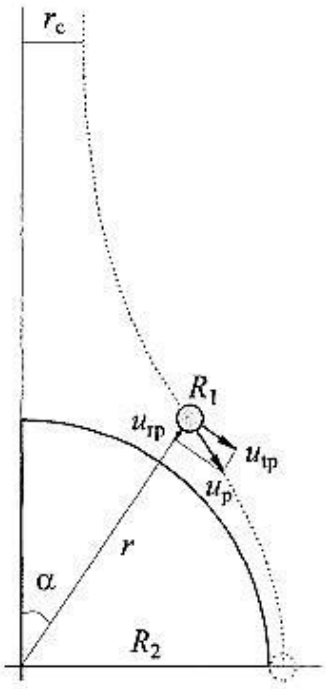

Figure 2-7: An illustration of streamline for particle of radius R_1 and air bubble of radius R_2 (Yoon and Mao, 1996)

The probability of collision (P) in equation 2.22 can be obtained by

$$P = P_c P_a (1 - P_d) \tag{2.36}$$

where P_c is the probability of bubble-particle collision, P_a is the probability of adhesion, and P_d is the probability of detachment. Analytical expressions for

these probability functions can be derived and substituted in equations 2.35 and 2.33 in order to find the first-order rate constant.

2.5.1 Probability of bubble-particle collision (P_c)

Assuming that the particle suspension is quiescent, while the bubble is rising up, the liquid around the bubble forms a number of streamlines. If the particles are small enough in order to be considered to have negligible inertia, then the particle trajectory will be known and consequently the probability of bubble-particle collision can be derived. The streamline functions can be derived from the solutions of Navier-Stokes equations. Yoon and Luttrell, 1989, derived an empirical stream function:

$$\Psi = u_2 R_2^2 \sin^2 \alpha \left[\frac{1}{2}x^2 - \frac{3}{4}x + \frac{1}{4x} + \frac{Re^{0.72}}{15}\left(\frac{1}{x^2} - \frac{1}{x} + x - 1\right)\right] \qquad (2.37)$$

where u_2 is the bubble rise velocity, x is the radial coordinate, r is the normalized bubble radius ($x = \frac{r}{R_2}$), α is the angular coordinate, and Re is the Reynolds number of the bubble.

As shown in figure 2.7, only those particles that are within the critical radius r_c will collide with the bubble, leading to the following expression for P_c:

$$P_c = \left(\frac{r_c}{R_1 + R_2}\right)^2 \qquad (2.38)$$

Combining equations 2.25 and 2.26 gives

$$P_c = \left[\frac{3}{2} + \frac{4Re^{0.72}}{15}\right]\left(\frac{R_1}{R_2}\right)^2 \qquad (2.39)$$

2.5.2 Probability of bubble-particle adhesion (P_a)

Figure 2.8 shows a diagram of bubble-particle interaction relating the potential energy (V) and the distance (H).

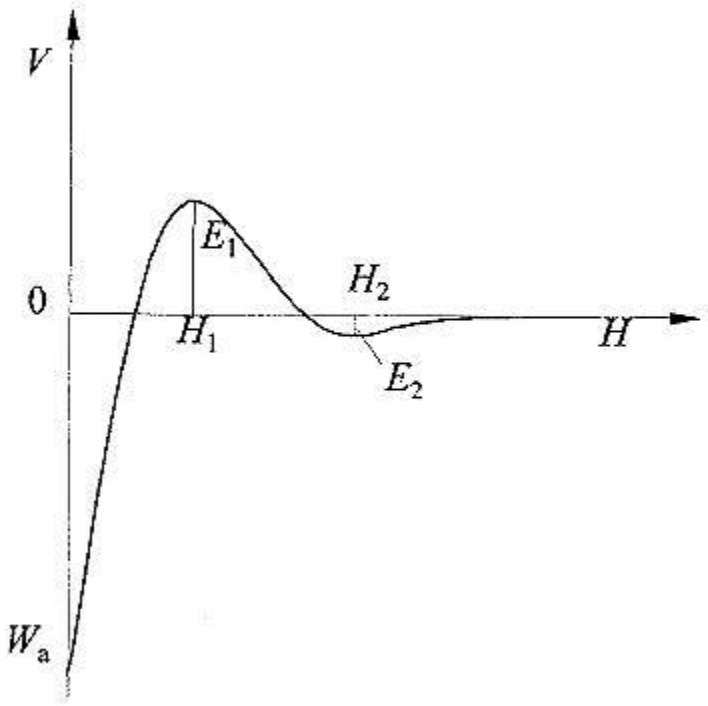

Figure 2-8: Potential energy vs. distance (Yoon and Mao, 1996)

In figure 2.8, E_1 is the energy barrier, E_2 is the secondary energy minimum and W_a is the work of adhesion. According to the DLVO theory, V is the sum of three interaction energies: (1) electrostatic (V_e), (2) dispersion(V_d), and (3) hydrophobic (V_h), therefore:

$$V = V_e + V_d + V_h \tag{2.40}$$

The expressions for each of these three interaction terms are

$$V_e = \frac{\epsilon R_1 R_2 (\Phi_1^2 + \Phi_2^2)}{4(R_1 + R_2)} [\frac{2\Phi_1 \Phi_2}{\Phi_1^2 + \Phi_2^2} \ln(\frac{1 + e^{-\kappa H}}{1 - e^{-\kappa H}})] \quad (2.41)$$

$$V_d = \frac{A_{123} R_1 R_2}{6H(R_1 + R_2)} [1 - \frac{1 + 2bl}{1 + \frac{bc}{H}}] \quad (2.42)$$

$$V_h = -\frac{R_1 R_2}{6(R_1 + R_2)} \frac{K_{123}}{H} \quad (2.43)$$

where ϵ is the dielectric constant of the medium, Φ_1 and Φ_2 are Stern potentials of the bubble and particle, $\frac{1}{\kappa}$ is the Debye length, A_{123} is the Hamaker constant of particle 1 and bubble 2 interacting in a medium 3, c is the velocity of light, and b and l are constants.

E_1 can be determined from V_e, V_d and V_h and therefore the expression for the probability of bubble-particle adhesion is

$$P_a = \exp(-\frac{E_1}{E_k}) \quad (2.44)$$

where E_k represents the kinetic energy of the macroscopic particles.

2.5.3 Probability of bubble-particle detachment (P_d)

Considering figure 2.8, when the kinetic energy exceeds the sum of the work of adhesion (W_a) and E_1, a particle could be detached from the surface of the bubble. Therefore, the probability of bubble-particle detachment is

$$P_d = \exp(-\frac{W_a + E_1}{E_k'}) \quad (2.45)$$

where E_k' represents the kinetic energy that makes the particles detach from the bubble surface.

Considering figure 2.9, the expression for the work of adhesion is

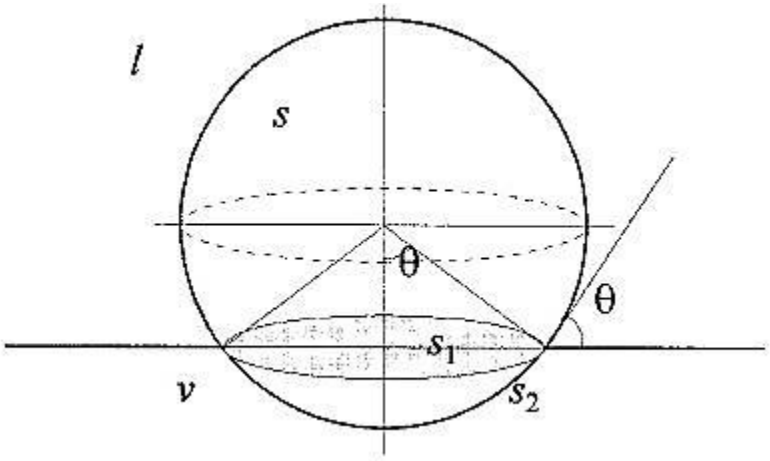

Figure 2-9: A spherical particle adhering on the surface of an air bubble (Yoon and Mao, 1996)

$$W_a = \gamma_{lv}\pi R_1^2(1 - cos\theta)^2 \tag{2.46}$$

where γ_{lv} represents the surface free energies at liquid/vapor interfaces, and θ is the contact angle.

Substituting equation 2.34 in equation 2.33 yields

$$P_d = \exp(-\frac{\gamma_{lv}\pi R_1^2(1 - cos\theta)^2 + E_1}{E_k'}) \tag{2.47}$$

Substituting equations 2.43, 2.44 and 2.46 in equation 2.35 and then equation 2.33 leads to the following expression for the first-order rate constant:

$$k = \frac{1}{4}S_b\left[\frac{3}{2} + \frac{4Re^{0.72}}{15}\right]\left(\frac{R_1}{R_2}\right)^2 \exp\left(-\frac{E_1}{E_k}\right)\left\{-\exp[-\frac{\gamma_{lv}\pi R_1^2(1 - cos\theta)^2 + E_1}{E_k'}]\right\} \tag{2.48}$$

Equation 2.48 relates the first-order rate constant to the hydrodynamic and surface chemistry parameters.

2.6 Kinetic models on flotation process

The models that are based on the axial dispersion theory rely on two main factors: (1) flotation kinetics, and (2) degree of mixing (Tuteja et al.,1994). For an impulse of tracer in a counter-current column, the mass transport equation is given by

$$D\frac{d^2C}{dx^2} - U_i\frac{dC}{dx} - \frac{dC}{dt} = 0 \tag{2.49}$$

where C is the concentration, D is the axial dispersion coefficient and x is the axial distance from the point of injection

The analytical solution of equation 2.37 is given by Wehner and Wilhelm, 1956:

$$Recovery\ (\%) = 100[1 - \frac{4\ a\ exp(\frac{1}{2N_P})}{(1+a^2)\exp\left(\frac{a}{2N_p}\right) - (1-a^2)\exp(-\frac{a}{2N_p})}] \tag{2.50}$$

where

$$a = \sqrt{1 + 4ktN_p} \tag{2.51}$$

and

$$N_p = \frac{D}{U_i L} \tag{2.52}$$

Assuming that there is plug flow in the system, N_p tends to zero and equation 2.50 becomes

$$Recovery = 1 - \exp(-kt) \tag{2.53}$$

If there is perfectly mixed flow in the system, N_p tends to infinity and equation 2.50 becomes

$$Recovery = \frac{kt}{1 + kt} \tag{2.54}$$

Other researchers, such as Finch and Dobby in 1990, proposed column flotation models based on the theory of axial dispersion. As an example, the overall recovery for a two-phase model is given by

$$Recovery = 100\frac{R_c R_f}{1 - R_c + R_c R_f} \tag{2.55}$$

where R_c represents the recovery for the collection zone and R_f the recovery for the froth zone.

2.7 Modelling of the froth zone recovery

An innovative methodology was developed by Vera et al.,2002, for modelling the froth zone recovery. Generally, the froth zone recovery depends on the residence time of particles in the froth which can be calculated using the froth retention time (FRT). FRT is the ratio of the froth volume to the volumetric flow rate of the concentrate. Gorain et al., 1998, have shown the relationship between the froth zone recovery and froth retention time, as shown in figure 2.10. The figure

indicates that the froth zone recovery is given by the following exponential function

$$f(a) = \exp(-\beta FRT) \tag{2.56}$$

where β is a parameter relating to coalescence of bubbles, which causes detachment and drainage.

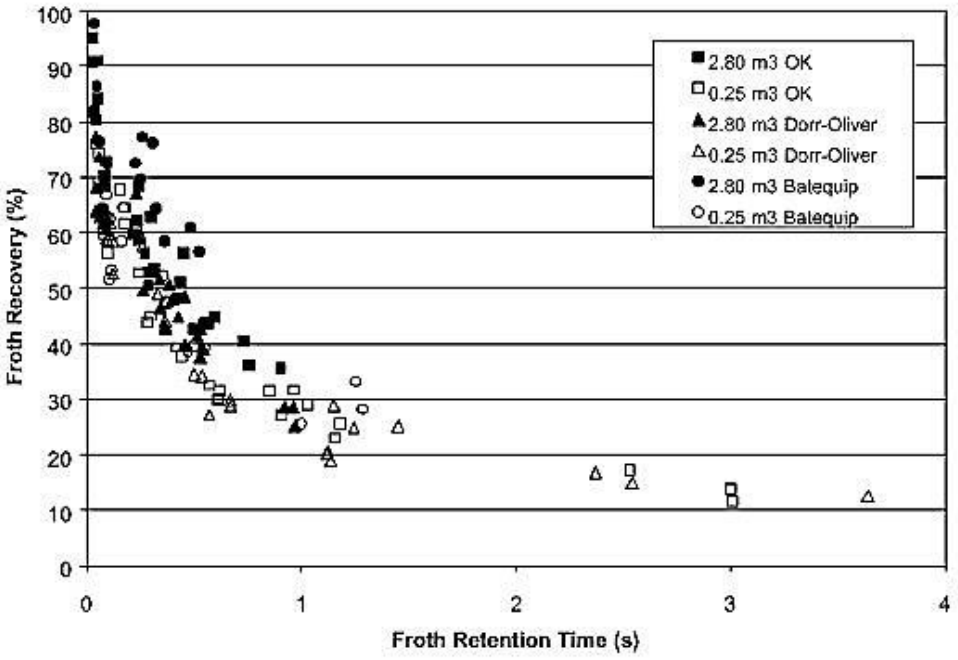

Figure 2-10: Froth zone recovery vs froth retention time (Vera et al., 2002)

Therefore, the detached particles, $(1 - f(a))$ may either drain back into the pulp phase or be recovered in the concentrate. Finally, by considering the drainage rate of detached particles, ω, the following expression is proposed (Mathe et al., 2000; Moys, 1989; Vera et al., 2002)

$$R_{fi} = \exp(-\beta FRT) + [1 - \exp(-\beta FRT)][\frac{1}{1 + \omega_i FRT}] \qquad (2.57)$$

2.8 Plateau border profile

By solving the differential equations 2.13 and 2.20 numerically, the profile of the Plateau border versus the height of the cell for both the regions, below the lip and over the lip, could be obtained. The region below the lip is an ordinary differential equation (ODE) Initial Value Problem (IVP) and the initial condition is given by

$$A_0 = A(y = 0) = \frac{\mathcal{E}_0}{\lambda} \tag{2.58}$$

The region above the lip is an ODE Boundary Value Problem (BVP) and the boundary conditions are given by

$$A\left(y = y_{lip}\right) = Constant \tag{2.59}$$

$$\frac{dA}{dy}\left(y = y_{overflow}\right) = 0 \tag{2.60}$$

where A_0 is the Plateau border area at the bottom of the cell and $\mathcal{E}_0$ is the liquid content at the bottom of the cell.

Finally, the equations were solved by using the finite difference method, and the results are shown in figures 2.11 and 2.12.

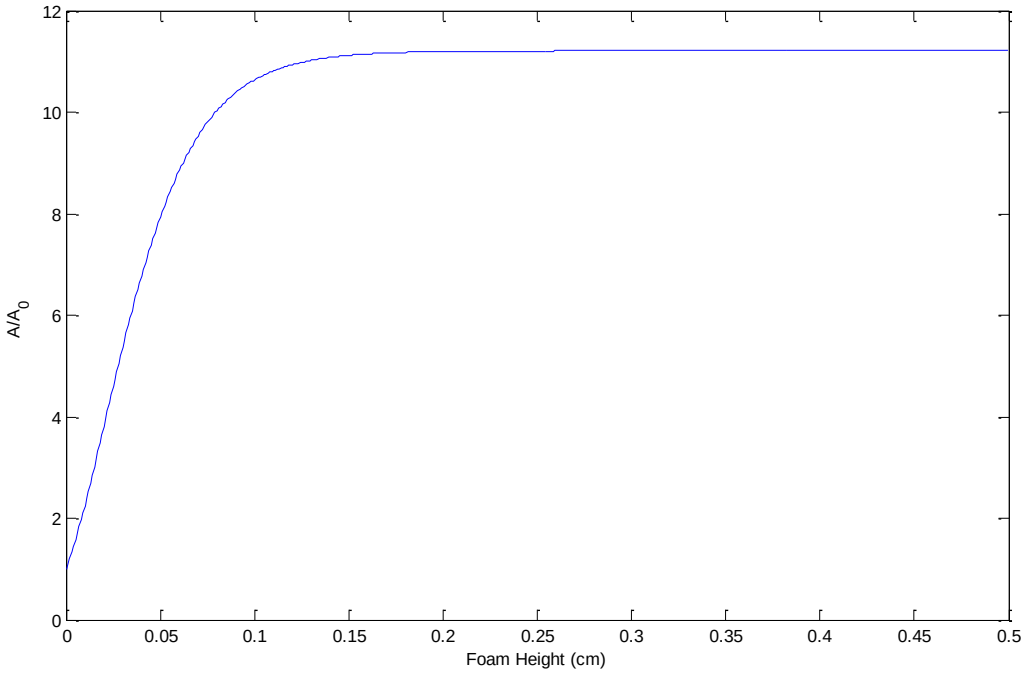

Figure 2-11: Plateau border profile for the region below the lip

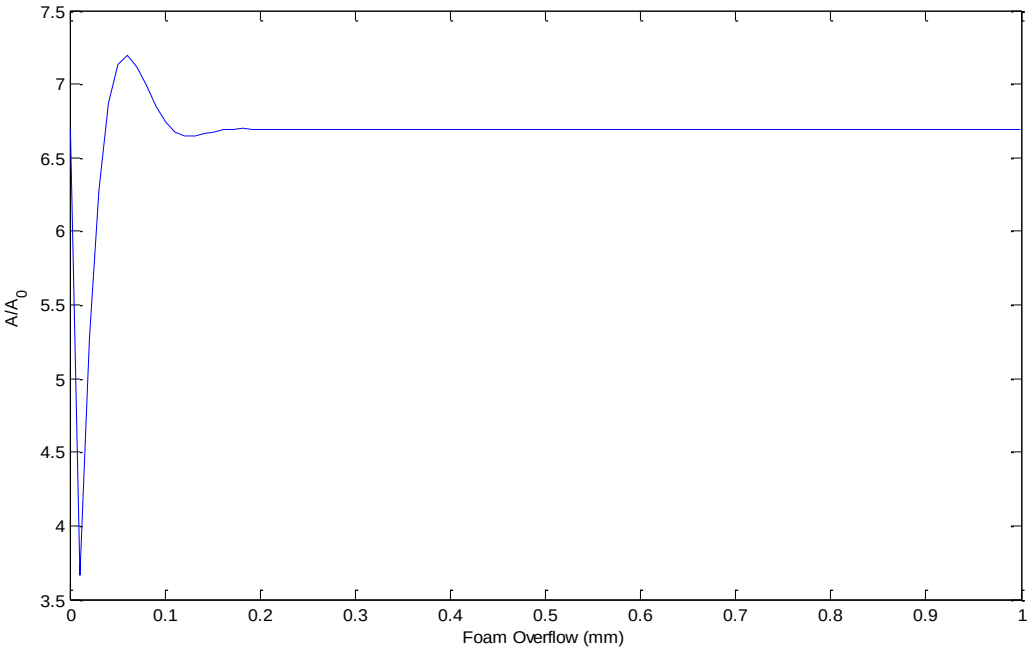

Figure 2-12: Plateau border profile for the region above the lip

Chapter 3

3 Experimental Design, Materials and Methods

This chapter contains a description of materials and reagents, experimental apparatus and setup and all of the procedures used in this study.

3.1 Chemicals

The three chemicals used as starting materials in the batch flotation cell were distilled water, pure Galena (the ore being floated), Potassium Ethyl Xanthate (KEX) as a collector and Methyl Isobutyl Carbinol (MIBC) as a frother.

Collectors are reagents that are used in flotation process in order to be absorbed selectively on the surface of particles, so that they can increase the contact angle and make it easier for the bubbles to adhere to the surface of particles. Frothers are used to stabilize the air bubbles during the flotation process, so the bubbles will remain well-dispersed in the pulp zone and are kept stable in the froth layer and do not burst before removal in the concentrate.

3.1.1 Galena

Pure Galena was obtained from Boreal Science Company in Canada in a cleavage form. According to the literature (McFadzean et al., 2013), in order for the Galena particles to reach a condition to be floated, their size should be less than 106 μm; therefore, 2 steps of crushing, using a jaw crusher and a disc pulverizer, were performed repeatedly to make the particles finer. After crushing with the disc pulverizer, the particles were analyzed using sieved particle size analysis to check

that all the particles passed the 106 µm sieve. Those that did not pass through the 106 µm sieve were put through the crushing steps again. Figure 3.1 describes the procedure of crushing the Galena ore in the laboratory in order to obtain the floatable size.

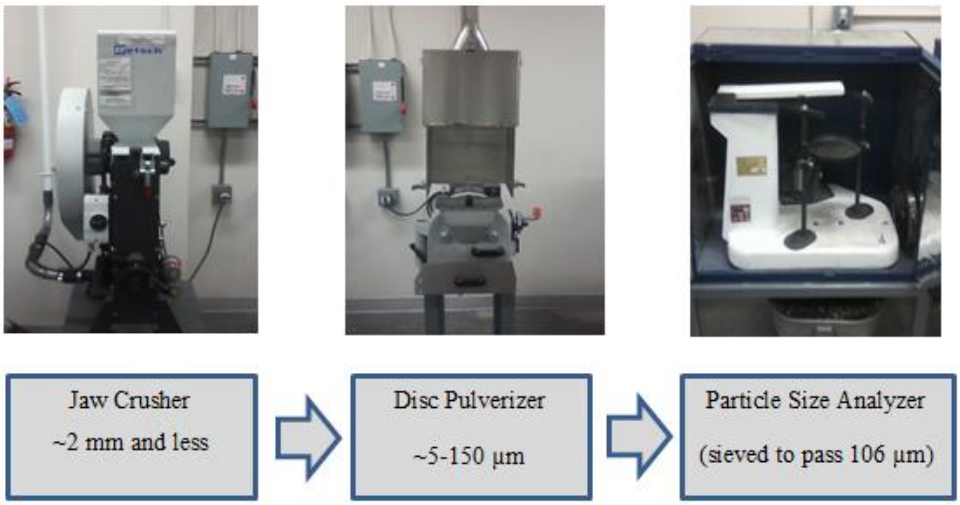

Figure 3-1: Procedure for crushing Galena

The results of the final particle size analysis of the Galena are reported in Table 3.1.

Table 3-1: Final particle size analysis of crushed Galena

Particle size (µm)	Weight %
106	0.8
75	4
45	59
38	7
<38	29.2

3.2 Batch flotation cell

The experiments were carried out in a JK Tech batch flotation cell with a capacity of 1.6 L equipped with a stirrer at the bottom of the cell. Images of the batch flotation cell are provided in figures 3.2 and 3.3. The stirrer obtains its power from a motor drive which is installed at the bottom of the cell. The air flow is sparged from the bottom of the cell by a tube which is connected to an existing air supply in the laboratory.

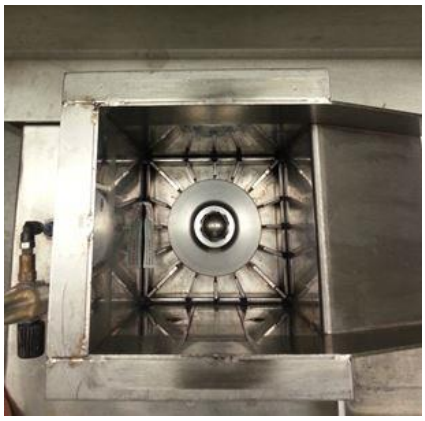

Figure 3-2: View of the batch flotation cell from the top

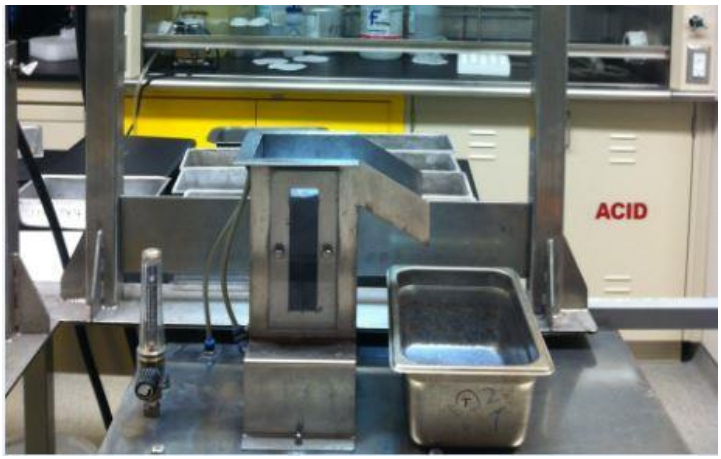

Figure 3-3: Side view of the batch flotation cell

3.3 Measurements & Image Processing

Visio-Froth is an image processing package for online measurements consisting of a camera and laser along with associated software. The camera is placed at the top of the cell and the laser is fixed with a calibration angle at the top corner of the floatation cell. The camera provides information about the top layer of the froth such as the velocity of the froth, bubble size distribution, color and froth characteristics (texture, stability and height), and the laser provides information about the height of the froth. A screen shot of the software is shown in figure 3.4, and an image of the complete experimental setup including the batch flotation cell, camera, laser and froth collection pans is given in figure 3.5.

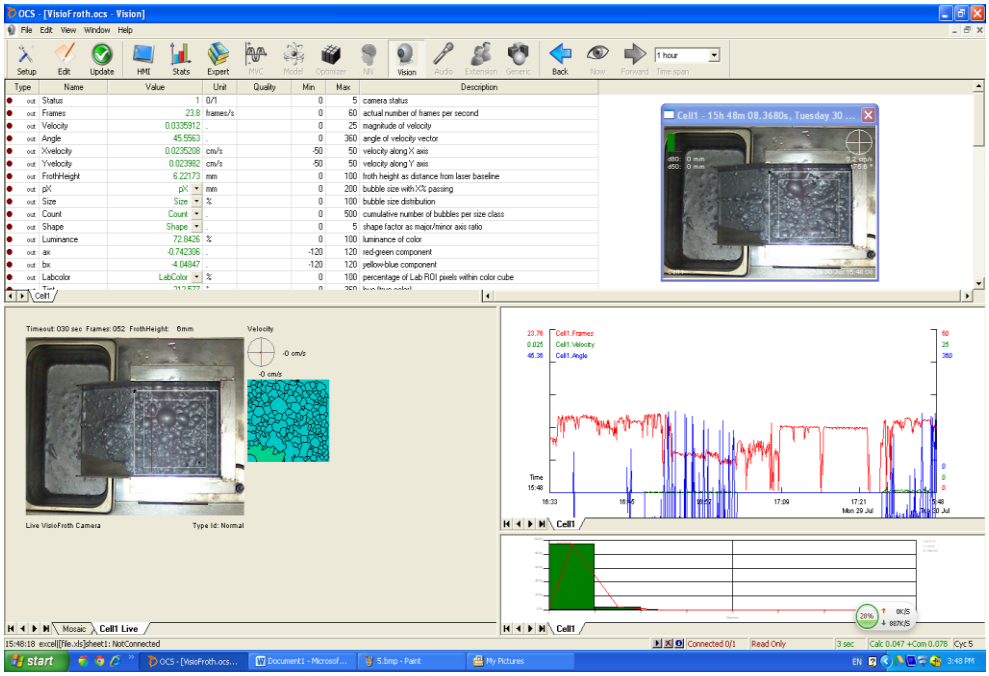

Figure 3-4: Screen shot of the image processing software

Figure 3-5: Complete flotation set-up including the cell and image processing equipment

3.4 Fractional Factorial Design (FFD) for flotation experiments

Fractional factorial design was used to investigate the relationship between the input variables and the output of the system (recovery), and to identify the significant process design variables. While 2^k factorial designs are required to analyze the effect of k factors, with 2 levels of each factor (Ogunnaike, 2011), using a fraction of the full design reduces the number of experiments at the cost of confounding some interaction effects. The output of the flotation process is the recovery which is believed to be dependent on the following four factors: (1) air flow rate, (2) impeller speed, (3) collector dosage and (4) frother dosage. Therefore; 2^4 runs, including all possible combinations of the factors, represent the full factorial design for this experiment. In this work, a 2^{4-1} design is chosen,

which requires 8 experiments. The high and low levels of the factors are specified in Table 3.2.

Table 3-2: Low and high levels of experimental factors

	Variables	Levels	
		-1	+1
A	Air flow rate (lit/min)	8	14
B	Impeller speed (rpm)	500	1100
C	Collector dosage (mol/lit slurry)	10^{-5}	10^{-3}
D	Frother dosage (ml/lit slurry)	0.042	0.1

If the 4 factors are designated A, B, C and D, the 2^{4-1} design is constructed by confounding the three-way interaction ABC with the factor D, i.e,

$$D=ABC \tag{3.1}$$

Table 3.3 details the experiments in the fractional factorial design.

Table 3-3: 2^{4-1} fractional factorial design

Run number	A	B	C	D	Recovery (%)
1	-1	-1	-1	-1	73.17
2	1	-1	-1	1	83.54
3	-1	1	-1	1	99.81
4	1	1	-1	-1	98.97

5	-1	-1	-1	-1	97.79
6	1	-1	1	-1	81.46
7	-1	1	1	-1	65.51
8	1	1	1	1	99.10

3.5 Experimental procedure

In the first step, 50 grams of Galena are placed in the batch flotation cell, to which distilled water is added to make up a volume of 1.4 L in the cell. In the second step, the specified amount of collector is added to the mixture and agitated for 8 minutes. After 8 minutes, in the last step, the frother is added to the system and then the mixture is agitated for another 2 minutes, at which point the flotation is started by turning on the air flow. At specified time intervals, the froth is collected in the overflow from the top of the cell and is saved in pans.

By using a vacuum filter, the water content of the pans is removed and the pans are placed in an oven (temperature: $500^{\circ}C$) for 5 hours to be dried. After 5 hours, the Galena that remains is weighed and the cumulative recovery is calculated. The calculated cumulative recovery results versus time are given in figure 3.6.

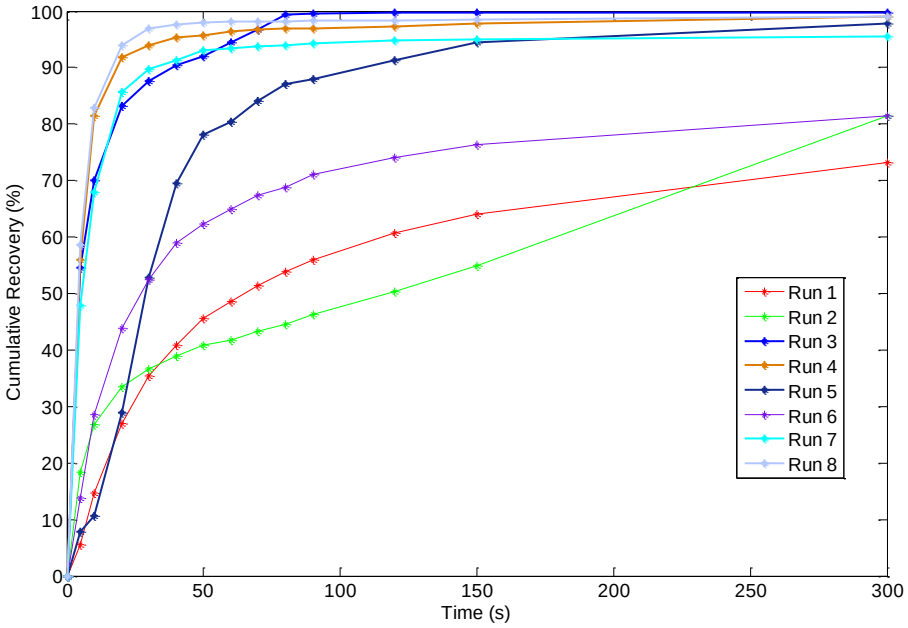

Figure 3-6: The calculated cumulative recovery for all 8 experiments

The responses of the recovery for the 2^{4-1} factorial design are provided in table 3.4.

Table 3-4: characteristics of half factorial design runs

Standard Order	Air flow rate (lit/min)	Impeller speed (rpm)	Frother dosage (ml(MIBC) per lit slurry)	Collecter dosage (mol(KEX) per lit slurry)	Recovery (%)
1	8	500	0.042	10^{-5}	73.17
2	14	500	0.042	10^{-3}	83.54
3	8	1100	0.042	10^{-3}	99.81
4	14	1100	0.042	10^{-5}	98.97
5	8	500	0.042	10^{-5}	97.79
6	14	500	0.1	10^{-5}	81.46
7	8	1100	0.1	10^{-5}	65.51
8	14	1100	0.1	10^{-3}	99.10

3.6 MINITAB analysis

Statistical analysis using MINITAB was conducted in order to determine which factor has in the greatest effect on the output of the system. In this analysis 3 kinds of outputs were considered: cumulative recovery, overall rate constant at t=50 seconds and overall rate constant at t=90 seconds. The reason for considering 2 outputs other than the cumulative recovery are to make it easier to distinguish the effects of the factors. Based on the 8 runs, the overall rate constant at the two specified time intervals was calculated and the results are given in Tables 3.5 and 3.6.

Table 3-5: Calculated overall rate constant at t=90 seconds

Run number	Residence time (s)	Recovery % at t=90s	Overall rate constant (1/s)
1	90	99.3	1.57
2	90	97	0.35
3	90	94.2	0.17
4	90	87.9	0.07
5	90	46.29	0.0094
6	90	98.2	0.54
7	90	71.02	0.027
8	90	55.90	0.013

Table 3-6: Calculated overall rate constant at t=50 seconds

Run number	Residence time (s)	Recovery % at t=50s	Overall rate constant (1/s)
1	50	0.92	0.23
2	50	0.95	0.38
3	50	0.93	0.26
4	90	0.78	0.07
5	50	0.40	0.013
6	50	0.97	0.64
7	50	0.62	0.048
8	50	0.45	0.024

According to figure 3.7 and Table 3.7 , factor B, impeller speed, is identified to have the largest absolute effect on the overall rate constant at t=50 seconds. It can also be concluded that the factor D, frother dosage, has the second largest effect on the rate constant at t=50 seconds. The results for the rate constant at t=90 seconds are given in Table 3.8 and figure 3.8. Factor B, the impeller speed, is identified again to have the most effect on this output and the frother dosage has the next largest effect. The results for cumulative recovery as the output are presented in Table 3.9 and figure 3.9, and the impeller speed again has the largest effect, followed by the frother dosage. The only issue in this analysis is that when the overall cumulative recovery is an output, it is hard to distinguish the significant factors due to the reason that the values of their effects are very close to each other. Therefore, it can be also concluded that when using the overall rate constant rather than recovery as the output is much better to distinguiush and analyze the effects of the factors in the experiments.

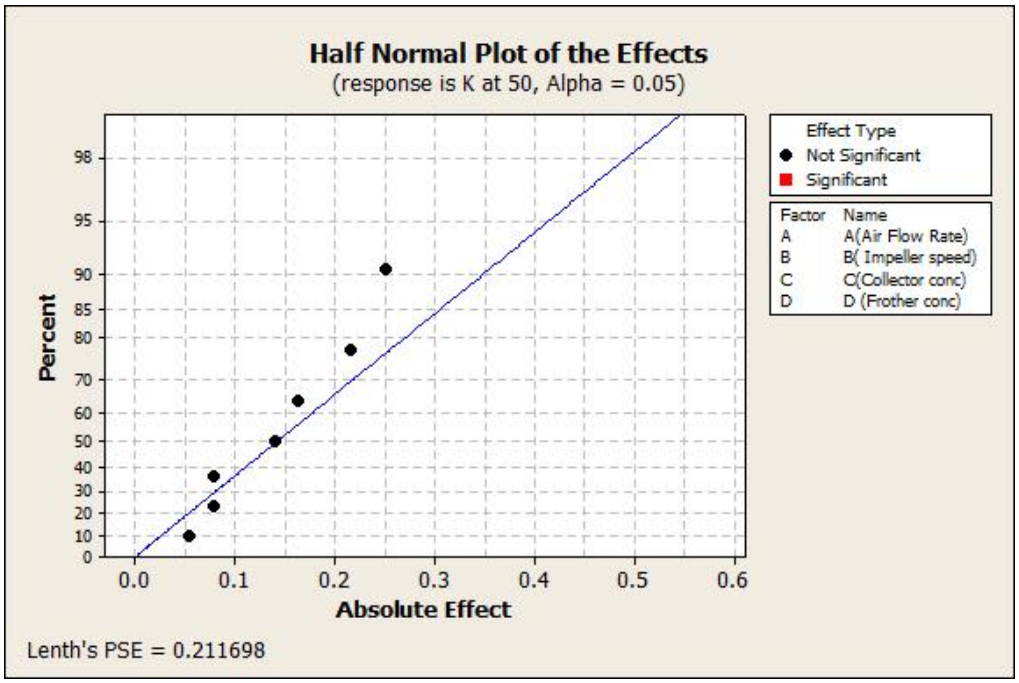

Figure 3-7: The probability plot for the effect when overall rate constant at t=50 se. is an output

Table 3-7: Estimated effects and coefficients for overall rate constant at t=50 se.

Term	Effect	Coefficient
Constant	--	0.2098
A	0.1411	0.0706
B	-0.2153	-0.1077
C	-0.0537	-0.0268
D	-0.0781	-0.0391
AxB	-0.2505	-0.1253
AxC	0.1635	-0.0818
AxD	-0.0787	-0.0393

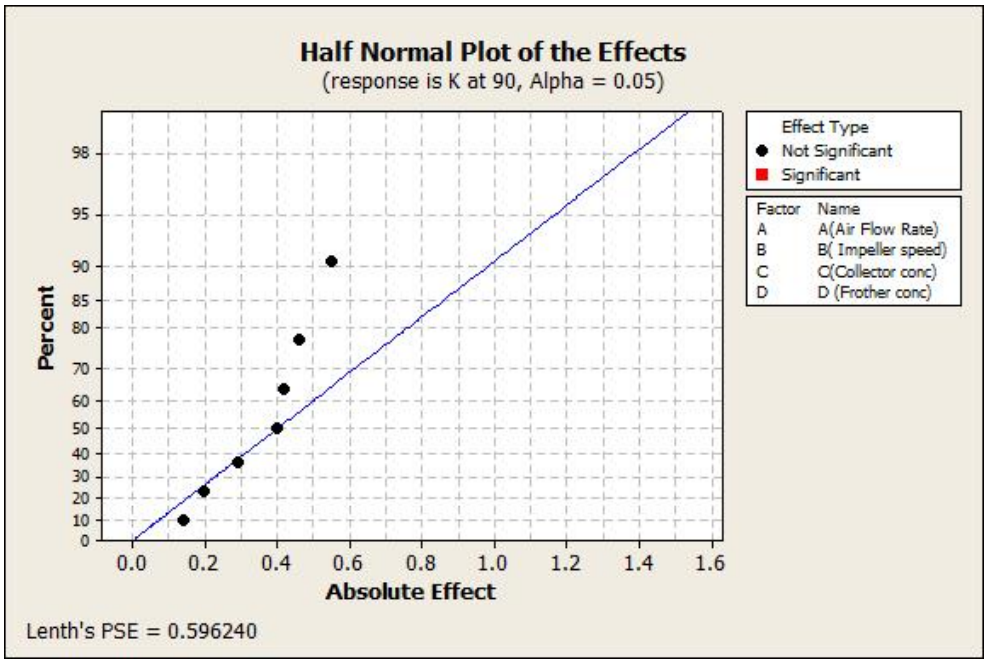

Figure 3-8: The probability plot for the effect when overall rate constant at t=90 se. is an output

Table 3-8: Estimated effects and coefficients for overall rate constant at t=90 se.

Term	Effect	Coefficient
Constant	--	0.3472
A	-0.1989	-0.0995
B	-0.5502	-0.2751
C	-0.3975	-0.1987
D	-0.4165	-0.2083
AxB	0.1421	0.0710
AxC	0.4594	0.2297
AxD	0.2933	0.1466

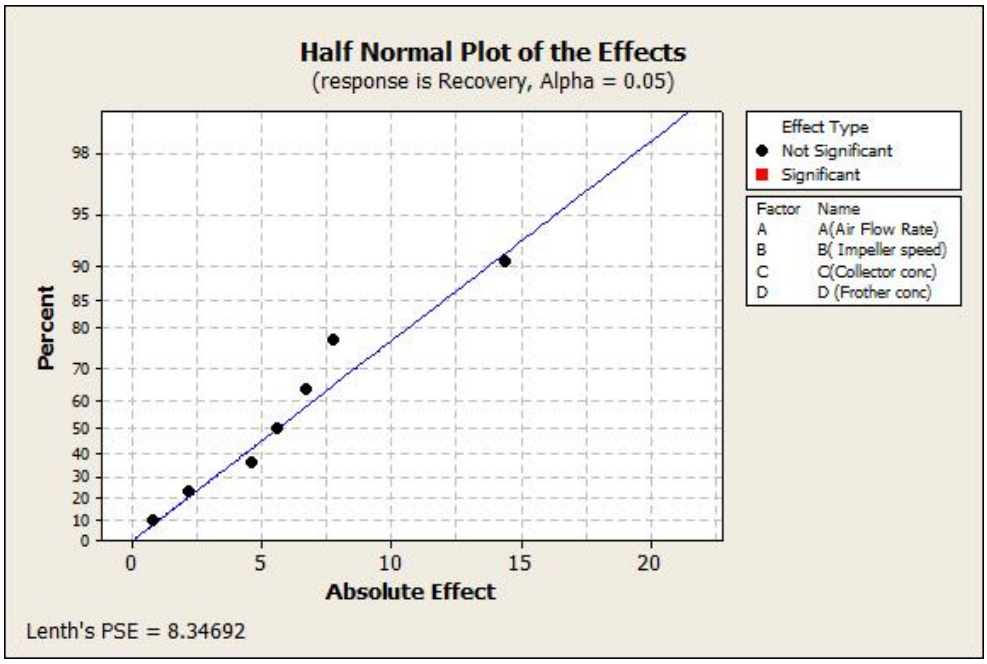

Figure 3-9: The probability plot for the effect when overall cumulative recovery is an output

Table 3-9: Estimated effects and coefficients for overall cumulative recovery

Term	Effect	Coefficient
Constant	--	91.170
A	-0.805	-0.403
B	14.355	7.178
C	4.590	2.295
D	7.780	3.890
AxB	2.180	1.090
AxC	-5.565	-2.783
AxD	-6.675	-3.337

Overall, there is no clear distinction in significant and non-significant factors in the analysis. However, as was mentioned previously, by comparing the values of the effects from the analysis, it can be concluded that the impeller speed and the frother concentration have the most effect (comparing to the other factors) in the final recovery of the mineral. In other words, it means these two paramters play significant roles in the performance of the flotation process.

3.7 Two-sample T-Test for comparing two sets of experiments

The froth flotation experiments were performed with two replicates. In order to decide whether the means of the two sets (populations) differ from each other or not, a two-sample T-Test was performed as described below.

- The sample means of both populations were calculated
- The sample standard Deviation (S) of both populations was calculated based on equation 3.2

$$S^2 = \frac{1}{n-1}\sum_{j=1}^{n}\left(x_j - \bar{x_j}\right)^2 \qquad (3.2)$$

- The T-value was calculated based on equation 3.3

$$t_{ij} = \frac{\bar{x_\iota} - \bar{x_j}}{\sqrt{\frac{S_1^2 + S_2^2}{n}}} \qquad (3.3)$$

- The degrees of freedom were calculated based on equation 3.4

$$df = n_1 + n_2 - 2 \qquad (3.4)$$

- The T-value was compared to the critical T-value
- Concluding whether the same experiments in two sets of runs are the same or not by comparing the calculated T-value and critical T-value from the

table. If the calculated one is greater than the critical one, then the two experiments are the same

The results are shown in table 3.10 and 3.11.

Table 3-10: Mean and standard deviation for two populations

	Population 1		Population 2	
Run	Mean ($\bar{X}$)	S^2	Mean ($\bar{X}$)	S^2
1	41.18545	491.6266	40.39908	495.9039
2	39.85744	495.9039	76.20356	339.3712
3	83.39402	339.3712	73.25536	710.3134
4	85.37903	710.3134	82.65214	748.2753
5	62.19804	748.2753	64.21911	712.3726
6	54.55561	712.3726	62.51799	729.5574
7	81.14875	729.5574	80.96643	629.1882
8	86.90552	629.1882	86.94816	1248.902

Table 3-11: T-Test result

Run	T_{value}	$T_{critical}$	Pass or fail
1	2.3658	1.706	✓
2	1.9854	1.706	✓
3	3.3658	1.706	✓
4	2.1478	1.706	✓
5	4.3698	1.706	✓
6	2.3258	1.706	✓
7	1.7236	1.706	✓
8	1.9632	1.706	✓

As it can be seen from the t-test results, all of the 8 runs passed the t-test which shows that there is no differences between the 8 runs in the first population and in the other replicate.

Chapter 4

4 Modelling and Parameter Estimation

4.1 Introduction

In 1960, R.E. Kalman proposed a recursive solution to solve some of the practical difficulties that arise when Weiner filters are applied. Since that time, the Kalman filter and its extensions have been widely used in recursive state and parameter estimation (Welch and Bishop, 2006).

The Kalman filter is an optimal estimator that consists of a set of mathematical equations that estimates the state of the process in a way that it minimizes the estimated error covariance. Consider a discrete-time linear stochastic state-space system with x ($x \epsilon R^n$) states and z ($z \epsilon R^m$) measurements:

$$x_k = A\,X_{k-1} + B\,U_{k-1} + w_{k-1} \tag{4.1}$$

$$Z_k = H\,x_k + v_k \tag{4.2}$$

where w_k and v_k represent the process and the measurement noise, respectively. They are white noise sequences with normal probability distributions:

$$p(w) \sim N(0, Q) \tag{4.3}$$

$$p(v) \sim N(0, R) \tag{4.4}$$

Q and R are the process noise covariance and measurement noise covariance, respectively.

4.1.1 The Extended Kalman Filter Algorithm

The equations for the Extended Kalman filter are divided to two groups: model prediction and measurement update equations. The Extended Kalman filter estimates the states of the process and then it receives the feedback in the form of measurements. The goal of model prediction equations is to obtain an a priori estimate for the next time step by estimating a current state and an error covariance based on the model. Then, for obtaining the a posteriori estimate, the measurement-update equations are used to update the a priori estimate. In other words, it can be said that the model prediction equations play the role of a predictor and the measurement-update equations play the role of a corrector. A schematic view of this algorithm, including the equations for prediction and correction is shown below in figure 4.1 (Welch and Bishop, 2006, Kalman, 1960).

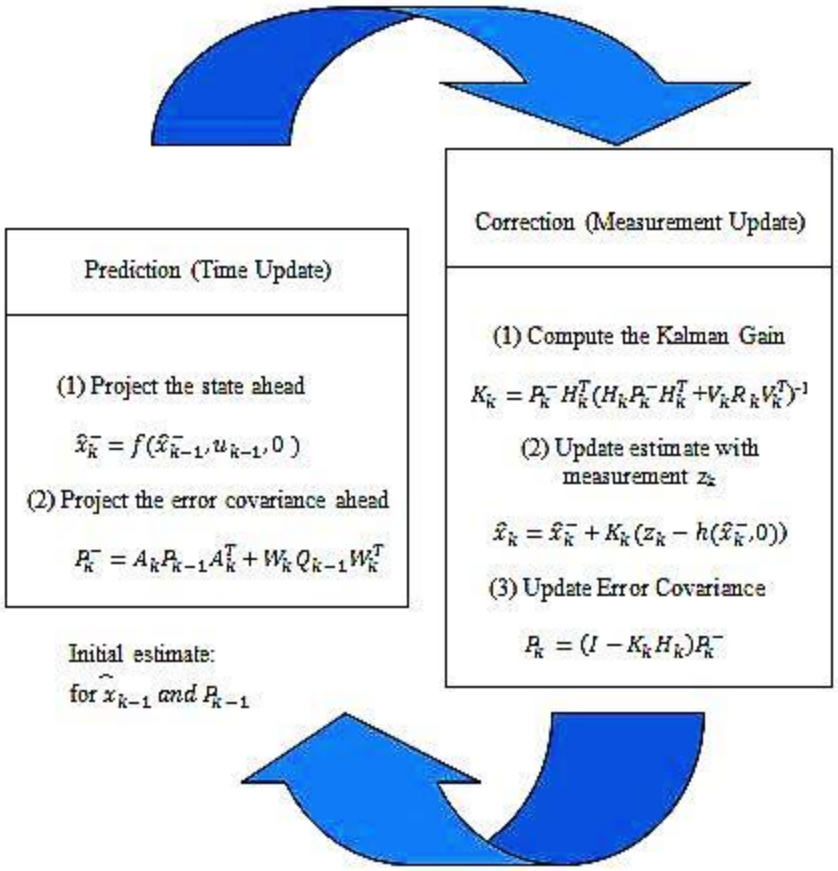

Figure 4-1: Discrete Extended Kalman filter algorithm (Welch and Bishop, 2006, Kalman, 1960)

In this study, the states and the parameters of the proposed model will continuously being estimated and updated online with the Extended Kalman Filter in order to provide an insight into fundamental physical processes and parameters governing the performance of flotation system.

4.2 Proposed Model

Since experimental studies are very expensive and time consuming, significant effort has been applied towards building mathematical models of the flotation

process; however, because of the complexity this process, the development of a fundamental flotation model based on the first principles has not been realized yet (Crozier, 1992; Bloom and Heindel, 2003). The proposed fundamental flotation framework in this research is based on the population balance, hydraulic forces, mass transfer and kinetic equations for attachment and detachment and entrainment/drainage between the defined three states (phases) flotation cell (Bascur, 2000). The model represents the existence of the mineralogical species at any time and at any of these three states. Each particle can be in any of these three states (phases): (1) particles that are free in the pulp, (2) particles that are attached to the bubbles in the pulp, (3) particles that are attached to the bubbles in the froth. Figure 4.2 represents the schematic mechanism of the model variables and mass transfer in the flotation cell.

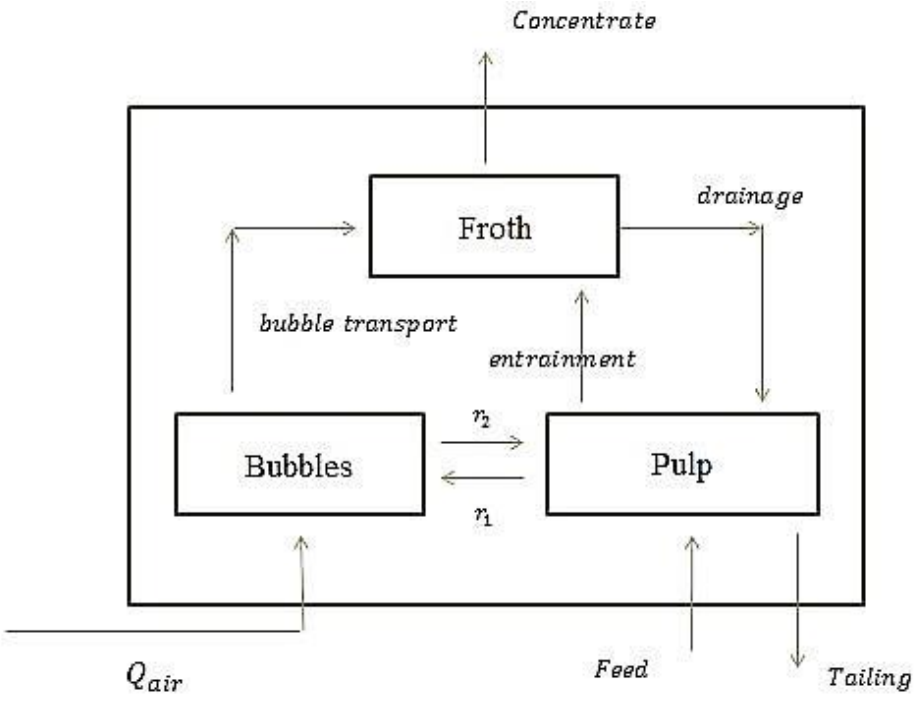

Figure 4-2: Schematic of general flotation framework

As can be seen in the figure 4.2, there are several mass transfer and kinetic processes between the three phases in the cell, such as selective attachment of mineral particles to the bubbles in the pulp phase (first order rate process), detachment of particles from bubbles in the pulp phase (first order rate process), transfer of particles that are attached to bubbles into the froth phase, transfer of hydrophilic particles from the pulp phase to the froth phase by entrainment, bubble coalescence in the froth phase, transfer of liquid (water) from the froth back to the pulp phase and drop-back of particles from the froth to the slurry. The proposed model can be described by a set of ordinary differential equations (ODEs) given by

$$\frac{d}{dt}\left(\varepsilon V_p x_b\right) = k_1(1-\varepsilon)V_p x_p - k_2 \varepsilon V x_b - Q_{air} x_b \tag{4.5}$$

$$\frac{d}{dt}\left((1-\varepsilon)V_p x_p\right) = k_2 \varepsilon V_p x_b - k_1(1-\varepsilon)V_p x_p - Q_E x_p + Q_{E'} x_c \tag{4.6}$$

$$\frac{d}{dt}\left(\varepsilon V_f x_c\right) = -k_3 V_f x_c - Q_{E'} x_c + Q_{air} x_b + Q_E x_p \tag{4.7}$$

where x_b is the concentration of particles on the surface of the bubbles in the pulp (kg/m^3), x_p is the concentration of particles free in the pulp (kg/m^3), x_c is the concentration of particles attached in the froth (kg/m^3), k_1 is the first order rate constant for attachment (s^{-1}), k_2 is the first order rate constant for detachment (s^{-1}), ε is the volume fraction of air, V_p is the volume of the pulp phase (m^3), V_f is the volume of the froth phase (m^3), Q_{air} is the air flow-rate (L/min), Q_E is the volumetric flow-rate of slurry from the pulp to the froth layer (L/min), $Q_{E'}$ is the volumetric flow-rate of liquid drainage from the froth layer to the pulp phase

(L/min) and Q_c is the volumetric flow-rate of product in the concentrate (L/min).

4.2.1 Attachment phenomena in the pulp phase

Following the work of Laskowsky, 1974, Yoon, 1999 and Jameson et el., 1997, the formation of bubble-particle aggregates in the pulp phase can be described in three significant steps: (1) approach of the particles to the surface of the bubbles, (2) thinning of the water layer between the particle and bubble, and (3) maintaining the air-solid interface by keeping the residual film between air and solid. Among the approaches for describing the attachment rate, Woodburn et al. 1971 and Bishofberger and Schubert, 1979, both derived an expression for the rate constant for attachment in which the phenomenon of turbulence was taken into consideration. Batchelor, 1953, did a comprehensive analysis on turbulence theory, and described turbulence by a statically continuous function that it is dependent on time and space, with velocity and pressure having irregular functions at a certain point in a turbulent field (Bascur, 2000). Therefore, the number of collisions per unit of volume and time in a flotation system, Z, in a flotation system is expressed by

$$Z = 5.0\, N_p N_B\, d_B^2\, U_t \tag{4.8}$$

where N_p is the number of particles ready for the collision, N_B is the number of bubbles ready for the collision, d_B is the mean size of the aggregates and U_t is the turbulent aggregate velocity (Bascur, 2000).

The observations of many researchers have shown that the flotation process can be visualized as a chemical reaction (Bloom and Heindel, 2003, Jameson, Nam, & Moo Young, 1977). The most general expression is proposed by Ahmed & Jameson, 1989:

$$\frac{dn_p^f(t)}{dt} = -k' \left(n_B^f(t)\right)^m \left(n_p^f(t)\right)^n \tag{4.9}$$

where $n_B^f(t)$and $n_p^f(t)$ are the concentrations of free bubbles and particles, respectively, t is the flotation time, k' is the pseudo-rate constant and m and n are the orders of the reaction with respect to bubbles and particles. The pseudo-rate constant can be expressed in the form of micro-process probabilities (Schulze, 1984, 1991, 1992; Bloom & Heindel, 1997a, b; Heindel, 1999; Julien Saint Amand, 1999; Heindel & Bloom, 2002) if the following assumptions are made: (1) the reaction is the first order (Woodburn, 1970; Ralston, 1992; Yoon & Mao, 1996; Nguyen, Ralston, & Schulze, 1998), (2) the bubble concentration is constant, and (3) the volume of the removed particles is negligible (Ahmed & Jameson, 1989) . Therefore; equation 4.9 can be written as:

$$\frac{dn_p^f(t)}{dt} = -k\, n_p^f(t) \tag{4.10}$$

where k is the rate constant and is expressed in the following form

$$k = Z\, P_c\, P_{asl}\, P_{tpc}\, P_{stab}\, n_B^f(t) \tag{4.11}$$

where Z is the bubble-particle collision frequency, P_c is the probability of bubble-particle collision, P_{asl} is the probability of bubble-particle attachment by sliding, P_{tpc} is the probability of forming a three-phase contact, P_{stab} is the probability of

bubble-particle aggregate remaining stable during the transfer from the pulp phase to froth phase and $n_B^f(t)$ is the concentration of bubbles without any particles attached to their surface (Bloom and Heindel, 2003).

The next step is to evaluate the bubble-particle collision frequency. The probability of bubble-particle collision, taken from the work of Heindel and Bloom (1999), is given by

$$P_c = \frac{1}{1+|G|}\left\{\frac{1}{2\left[\frac{R_p}{R_B}+1\right]^3)}\left[2\left(\frac{R_p}{R_B}\right)^3+3\left(\frac{R_p}{R_B}\right)^2\right]\right.$$

$$\left.+\frac{2Re_B^*}{\left[\frac{R_p}{R_B}+1\right]^4}\left[\left(\frac{R_p}{R_B}\right)^3+2\left(\frac{R_p}{R_B}\right)^2\right]\right\}+\frac{|G|}{1+|G|} \quad (4.12)$$

where R_p and R_B are the particle and bubble radius, respectively. G is the dimensionless particle settling velocity and is defined as

$$G = \frac{\upsilon_{ps}}{\upsilon_B} \quad (4.13)$$

where υ_{ps} is the particle settling velocity and υ_B the bubble rise velocity (Bloom and Heindel, 2003).Also,

$$Re_B^* = \frac{1}{15}\, Re_B^{0.72} \quad (4.14)$$

$$Re_B = \frac{\rho_l\, \upsilon_B\, d_B}{\mu_l} \quad (4.15)$$

where Re_B is the bubble Reynolds number, number, μ_l is the liquid dynamic viscosity, ρ_l is the liquid density and d_B is the bubble diameter. The probability of attachment by sliding is expressed as (Bloom and Heindel, 1999)

$$P_{asl} = exp\left\{-2\left(\frac{\tilde{\lambda}}{C_b}\right)\left(\frac{R_p}{R_p + R_b}\right)\left(\frac{g(r) - G}{|k(r)| - G}\right)\left(\frac{h_0}{h_{crti}} - 1\right)\right\} \tag{4.16}$$

where

$$g(r) = \left(1 - \frac{3R_b}{4r} - \frac{R_b^3}{4r^3}\right) + Re_b^*\left(\frac{R_b}{r} + \frac{R_b^3}{r^3} - \frac{2R_b^4}{r^4}\right) \tag{4.17}$$

$$k(r) = -\left\{\left(1 - \frac{3R_b}{2r} + \frac{R_b^3}{2r^3}\right) + 2Re_b^*\left(\frac{R_b^4}{r^4} - \frac{R_b^3}{r^3} - \frac{R_b^2}{r^2} + \frac{R_b}{r}\right)\right\} \tag{4.18}$$

$$\tilde{\lambda} = \frac{6\pi\mu_l R_p}{f} \tag{4.19}$$

where $r \sim R_B + R_P$, f is the fluid friction factor, C_B is a constant representing the bubble surface mobility, h_0 is the initial thickness of the film at the time the sliding process begins and the particle starts to contact the bubble and h_{crit} is the liquid film thickness at the time that the film starts to rupture (Bloom and Heindel, 2003).

The probability of forming a three-phase contact (P_{tpc}) is assumed to be approximately 1 (i.e., highly probable), following the work of Bloom and Heindel, 2002).

The probability of stability (P_{stab}) is defined as (Schule, 1993)

$$P_{stab} = 1 - exp\left(1 - \frac{1}{Bo'}\right) \tag{4.20}$$

$$Bo' = \frac{4R_p^2\left(\Delta\rho_p g + \frac{\left(1.9\rho_p \varepsilon^{\frac{2}{3}}\right)}{\left(R_p + R_b\right)^{\frac{1}{3}}}\right) + 3R_p\left(\frac{2\sigma}{R_b} - 2R_b\rho_l g\right) sin^2\left(\pi - \frac{\theta}{2}\right)}{\left|6\sigma \sin\left(\pi - \frac{\theta}{2}\right)\sin\left(\pi + \frac{\theta}{2}\right)\right|} \tag{4.21}$$

where ϵ is the Kolmogorov turbulent energy density, g is the gravity acceleration, θ is the contact angle, ρ_p is the particle density and $\Delta\rho_p = (\rho_p - \rho_l)$ (Bloom and Heindel, 2003).

Finally, the bubble-particle collision frequency can be written as

$$Z = 5\left(R_b + R_p\right)^2\sqrt{U_p^2 + U_b^2}\, exp\left[-\frac{1}{2}\frac{\left(\left|v_{ps}\right| + v_b\right)^2}{U_p^2 + U_b^2}\right] +$$

$$+\pi\left(R_b + R_p\right)^2 erf\left\{\frac{\left(\left|v_{ps}\right| + v_b\right)^2 + U_p^2 + U_b^2}{\sqrt{2(U_p^2 + U_b^2)}}\right\} \tag{4.22}$$

where

$$U_p = 0.4\frac{\varepsilon^{\frac{4}{9}} d_p^{\frac{7}{9}}}{v_l^{\frac{1}{3}}}\left(\frac{\rho_p - \rho_l}{\rho_l}\right)^{\frac{2}{3}} \tag{4.23}$$

$$U_b = 0.4\frac{\varepsilon^{\frac{4}{9}} d_b^{\frac{7}{9}}}{v_l^{\frac{1}{3}}}\left(\frac{\rho_b - \rho_l}{\rho_l}\right)^{\frac{2}{3}} \tag{4.24}$$

4.2.2 Detachment phenomena in the pulp phase

Bloom and Heindel (1977a, b, 2003) developed a population balance model to include both attachment and detachment phenomena that can be considered as the equivalents of forward and reverse reactions:

$$\frac{dn_p^f(t)}{dt} = -k_1 n_p^f(t) + k_2\, n_B^a(t) \tag{4.25}$$

where $n_B^a(t)$ is the concentration of the bubbles to which particles are attached on their surface, k_1 is the attachment rate constant and k_2 is the detachment rate constant. The first term in equation 4.25 represents attachment phenomena by the formation of bubble-particle aggregates and the second term represents detachment phenomena in which the aggregates become unstable and do not reach the froth layer (Bloom and Heindel, 2003). The detachment rate constant is expressed as

$$k_2 = Z' P_{destab} = Z'(1 - P_{stab}) \tag{4.26}$$

where Z' is the detachment frequency and P_{destab} the probability of the bubble-particle aggregate becoming unstable in the pulp phase. The expression for Z' is

$$Z' = \frac{\sqrt{C_1}\varepsilon^{\frac{1}{3}}}{\left(d_p + d_b\right)^{\frac{2}{3}}} \tag{4.27}$$

where C_1 is an empirical constant taken as 2 (Bloom and Heindel, 2003).

The rate of attachment, k_1, can be calculated by substituting equations 4.12, 4.16, 4.20 and 4.22 in equation 4.11. Also, k_2 , the rate of detachment, can be calculated by substituting equations 4.20 and 4.27 in equation 4.26. The rates of

attachment and detachment are then used in the differential equations 4.5, 4.6 and 4.7 to simulate the flotation process, leading to the calculation of the amount of valuable mineral in the three regions in the flotation cell with time.

4.3 State Space Model

For parameter estimation and online updating of the proposed model, the three differential equations are expressed in state-space format. The states and the output are given by

$$[\dot{x}] = [A]x + [B]U \tag{4.28}$$

$$\begin{bmatrix}\dot{x}_1\\ \dot{x}_2\\ \dot{x}_3\end{bmatrix} = \begin{bmatrix}-a_1 & a_2 & 0\\ a_3 & -a_4 & a_5\\ a_7 & 0 & -(a_8+a_9)\end{bmatrix}\begin{bmatrix}x_1\\ x_2\\ x_3\end{bmatrix} + \begin{bmatrix}0\\ a_6\\ 0\end{bmatrix} \tag{4.29}$$

$$y = [0 \quad 0 \quad \frac{\epsilon\, V_f t_{samp}\, k_3}{m_{init}}]\begin{bmatrix}x_1\\ x_2\\ x_3\end{bmatrix} \tag{4.30}$$

where y is the percentage recovery, m_{init} is the initial mass material in the batch flotation cell and k_3 is the rate of removal material in the concentration product ($\frac{1}{s}$). x_1 , the first state, is the mass of solids attached to the bubbles per volume of pulp phase ($\frac{kg}{m^3}$), x_2, the second state, is the mass of solids free in pulp phase per volume of pulp phase ($\frac{kg}{m^3}$) and x_3 , the third state, is the mass of solids attached to the bubbles in the froth phase. The input for the current state-space model is the air flowrate. The parameters of the proposed state space model are given in Table 4.1.

The next involves offline estimation of model parameters based on the 8 batch flotation runs.

Table 4-1: Parameters in the state space model

Parameter	Definition
a_1	$k_2 + \frac{Q_{air}}{\epsilon\, V_p}$
a_2	$\frac{k_1(1-\epsilon)}{\epsilon}$
a_3	$\frac{k_2\,\epsilon}{(1-\epsilon)}$
a_4	k_1
a_5	$\frac{Q_E}{(1-\epsilon)V_p}$
a_6	$\frac{\dot{m}}{(1-\epsilon)V_p}$
a_7	$\frac{Q_{air}}{\epsilon V_f}$
a_8	$\frac{Q_E}{\epsilon V_f}$
a_9	$\frac{k_3}{\epsilon}$

4.4 Offline Parameter Estimation

This section describes the fitting of the model to the experimental data obtained from the batch flotation tests. In each run the operational conditions of the experiments are input into the model and the states and the final recovery are calculated and then the results are compared with the experimental data. The function 'fmincon' in Matlab is used to find the best values of the parameters

$(k_1, k_2, k_3\ and\ \epsilon)$ that result in the lowest error between the model predictions and experimental values for the cumulative recovery. The results for these 8 simulations are given from figure 4.3 to 4.10.

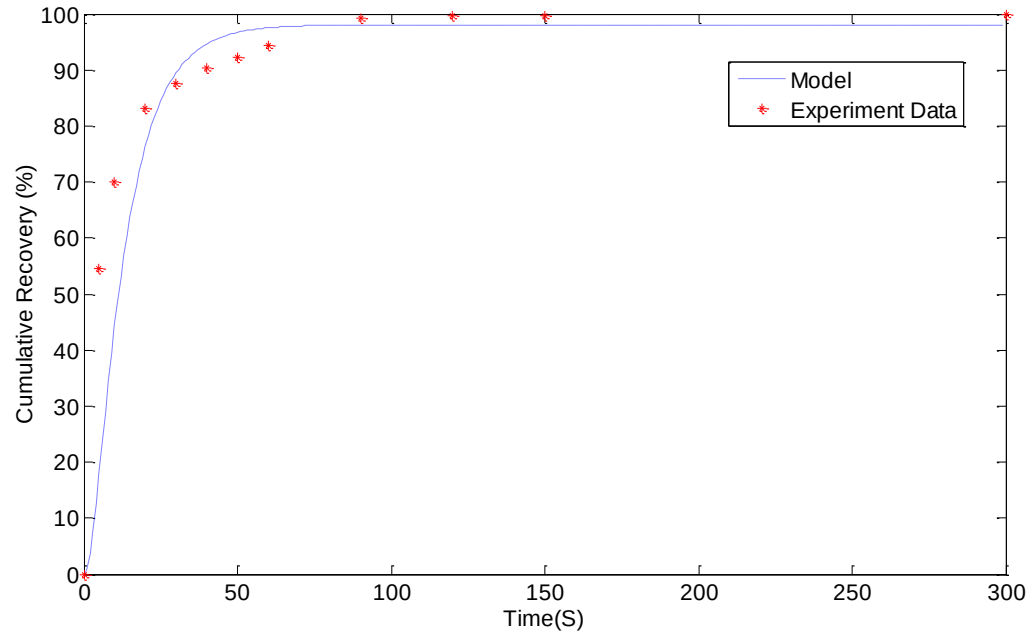

Figure 4-3: Comparing model predictions with experimental data for run 1

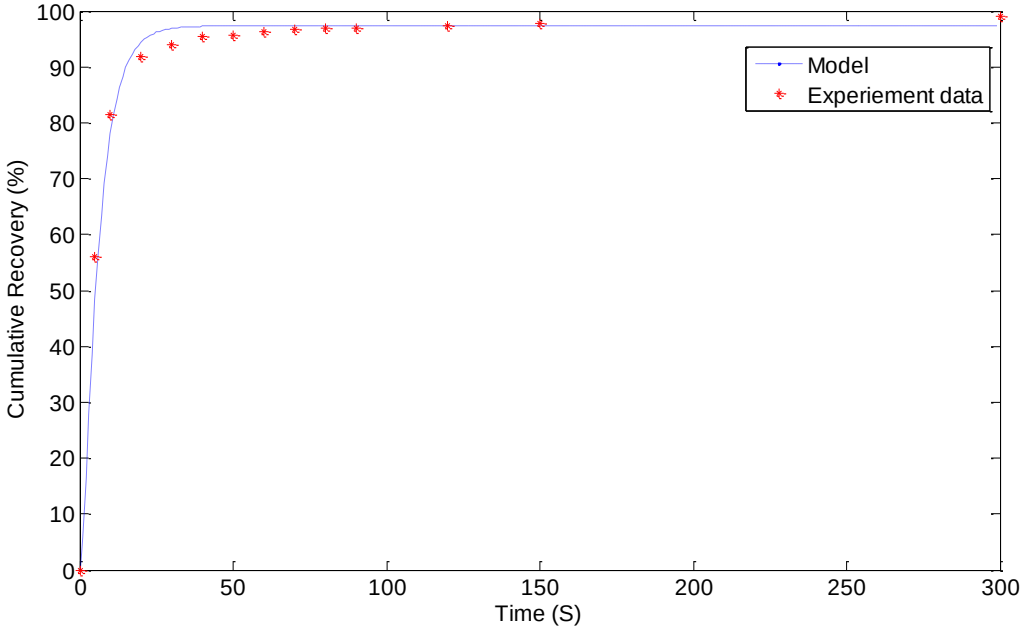

Figure 4-4: Comparing model predictions with experimental data for run 2

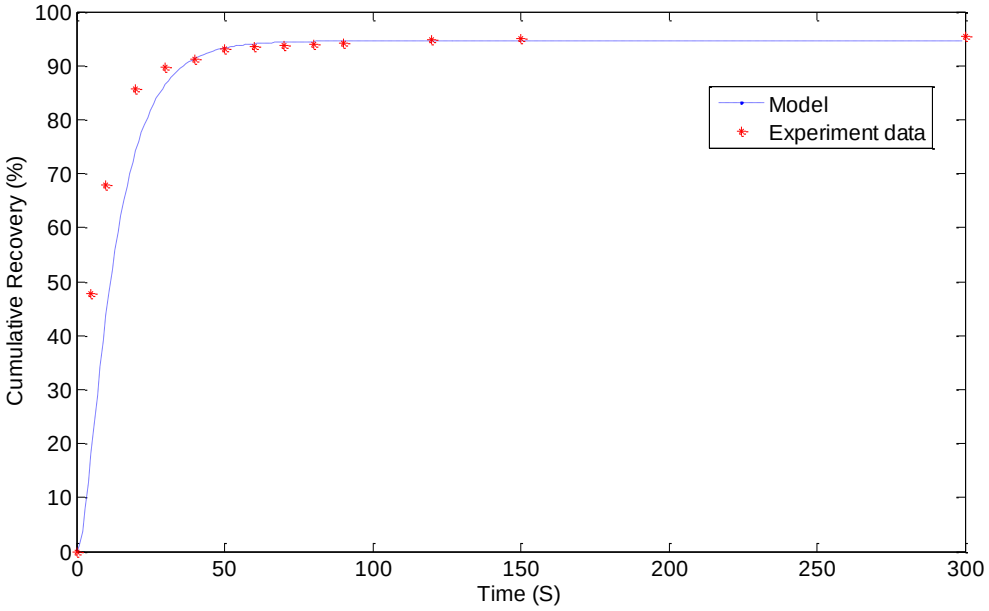

Figure 4-5: Comparing model predictions with experimental data for run 3

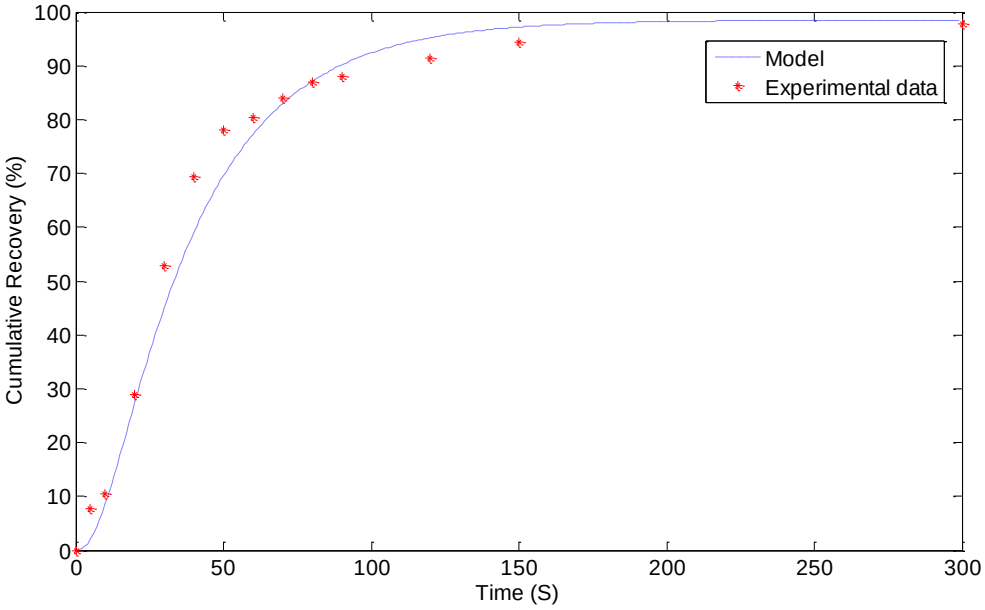

Figure 4-6: Comparing model predictions with experimental data for run 4

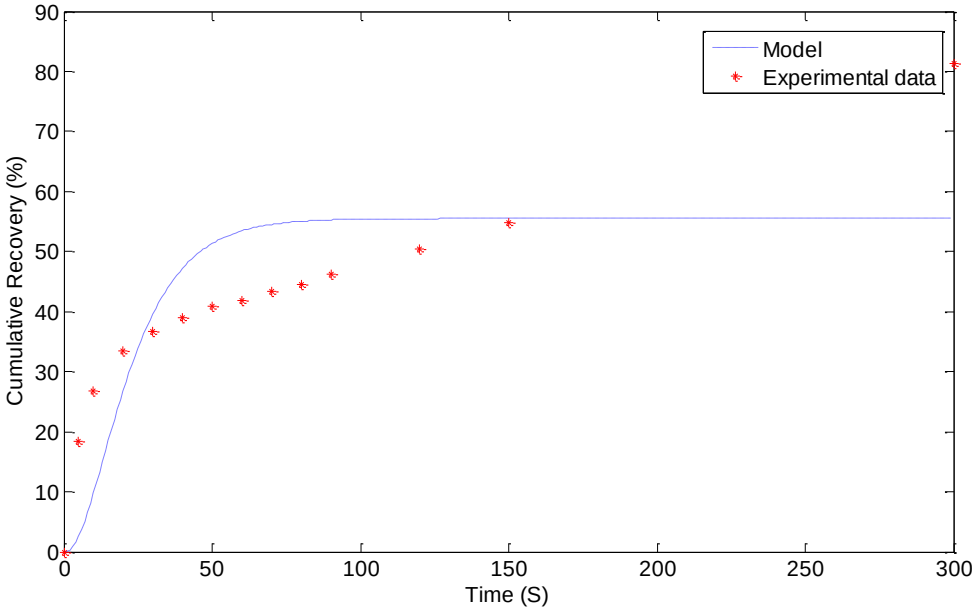

Figure 4-7: Comparing model predictions with experimental data for run 5

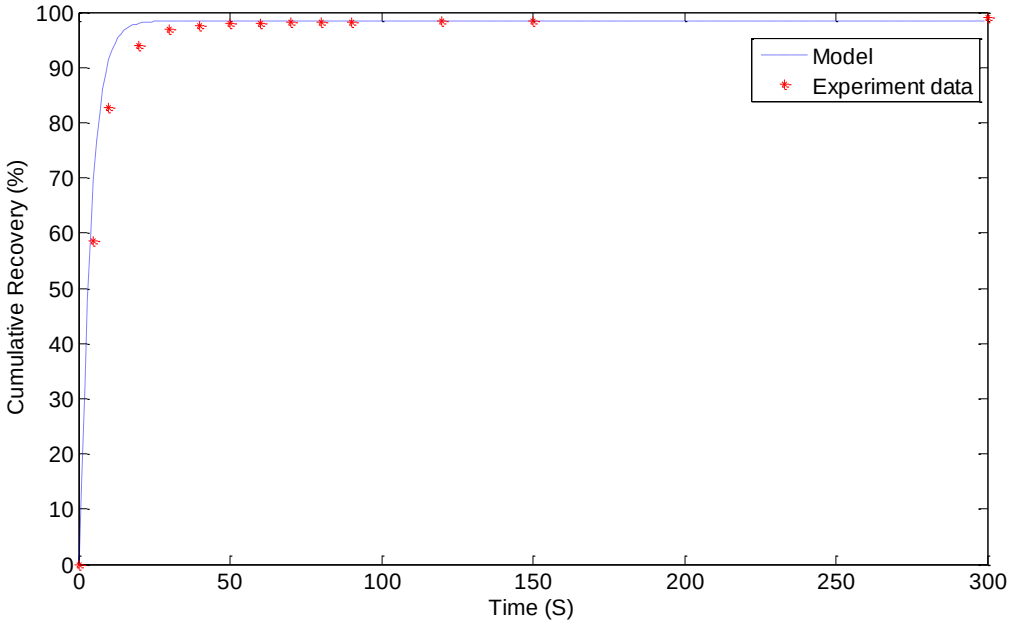

Figure 4-8: Comparing model predictions with experimental data for run 6

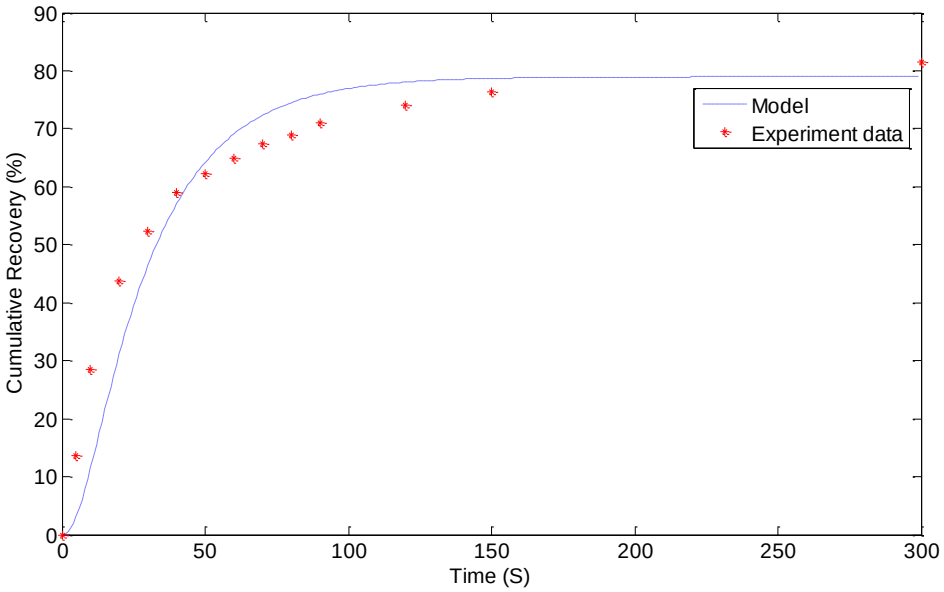

Figure 4-9: Comparing model predictions with experimental data for run 7

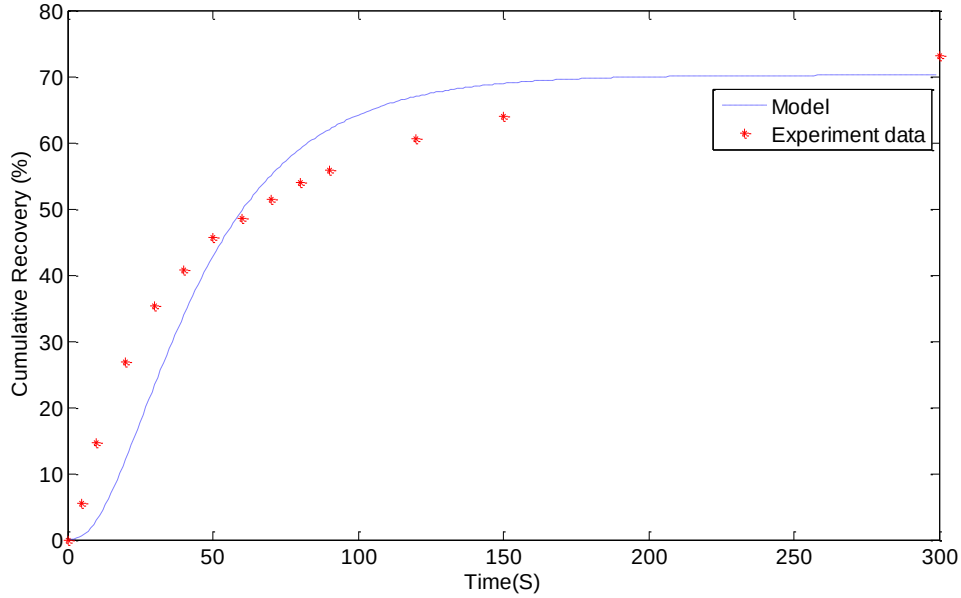

Figure 4-10: Comparing model predictions with experimental data for run 8

4.5 Real-Time Updating of the Model Parameters Using EKF

Two runs were selected for predicting the recovery, estimating and updating of the states and parameters of the system using the Extended Kalman Filter (EKF), run number 1 and run number 8. As there is only one measurement in the system (recovery), besides estimating the 3 states in the Kalman filter estimator, observability conditions indicate that only one parameter can be estimated and updated online. The three parameters that are desirable to be estimated and updated online are k_1, k_2 and k_3. The rest are operational variables such as the air flow rate that remained constant in each run. Therefore, three filters were run in parallel, with each one updating one of the parameters. These are three possible solutions to the parameter estimation problem. The parameter estimates for run 1 are given in table 4.2 and for run 8 in table 4.3.

Table 4-2: Model parameters

Parameter	Value	Remarks
Air flow rate (lit/min)	8	Constant
V_p (m^3)	$1.4\ x\ 10^{-3}$	Constant
V_f (m^3)	$0.26\ x\ 10^{-3}$	Constant
ϵ	0.4	Constant
k_1 ($\frac{1}{S}$)	Final value=48.3	Estimated and updated in simulation no. 1
k_2 ($\frac{1}{S}$)	Final value=23.54	Estimated and updated in simulation no. 2

$k_3\ (\frac{1}{S})$	Final value=13.33	Estimated and updated in simulation no. 3

Estimating the three parameters (k_1, k_2 and k_3), were performed in parallel for each experiment. In each run, one of the parameters would be estimated and updated online in the model and simultaneously the cumulative recovery of the system was predicted and updated. Figure 4.11 to 4.16 show the results for estimating the parameters and the cumulative recovery for run number 1. As it could be seen in the results, by updating the parameters and the states of the system online, the model could catch the dynamic of the system very well. The same procedure was done for run number 8. The results are shown in figure 4.17 to 4.22.

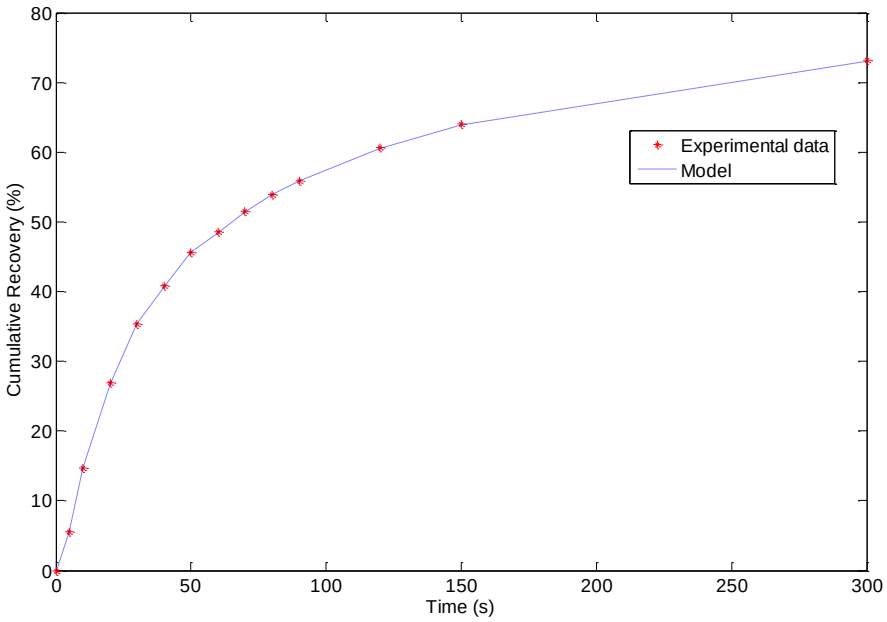

Figure 4-11: Comparing model predictions (based on the Kalman filter) with experimental data while parameter k_1 is being updated

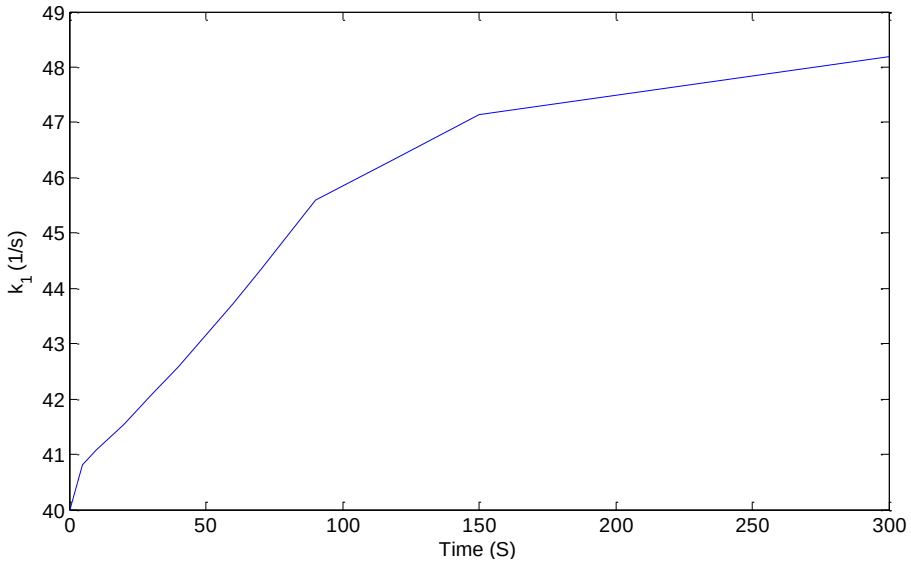

Figure 4-12: Estimate of parameter k_1 with time

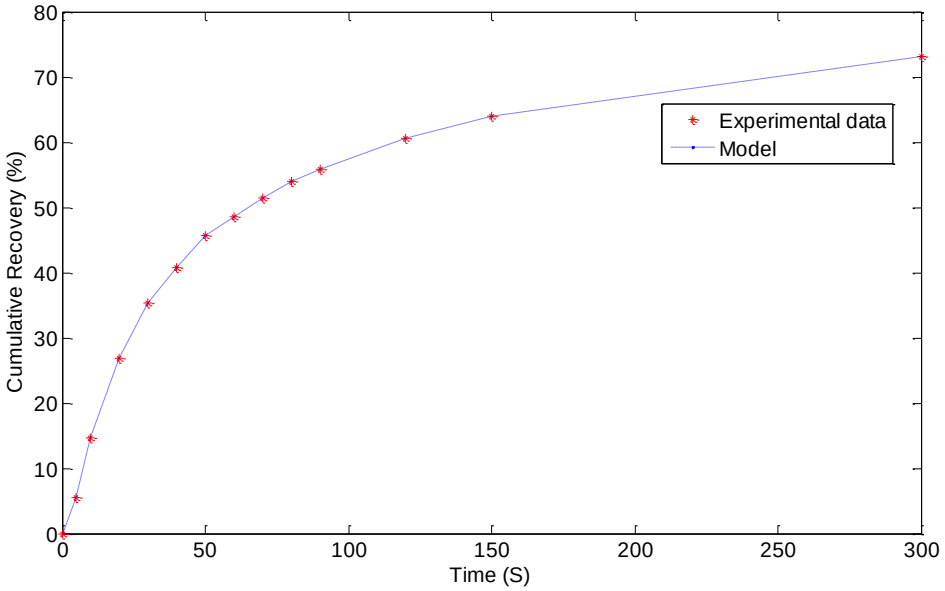

Figure 4-13: Comparing model predictions (based on the Kalman filter) with experimental data while parameter k_2 is being updated

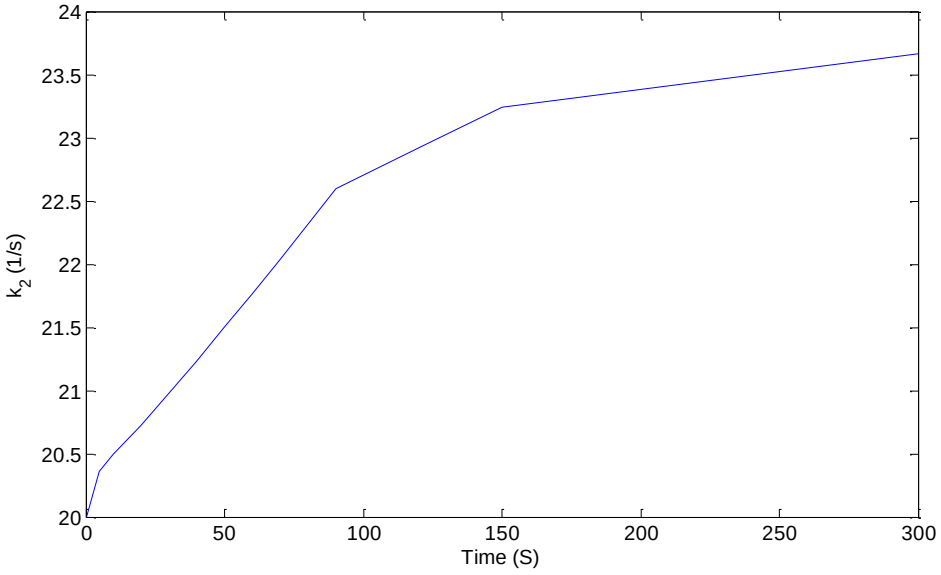

Figure 4-14: Estimate of parameter k_2 with time

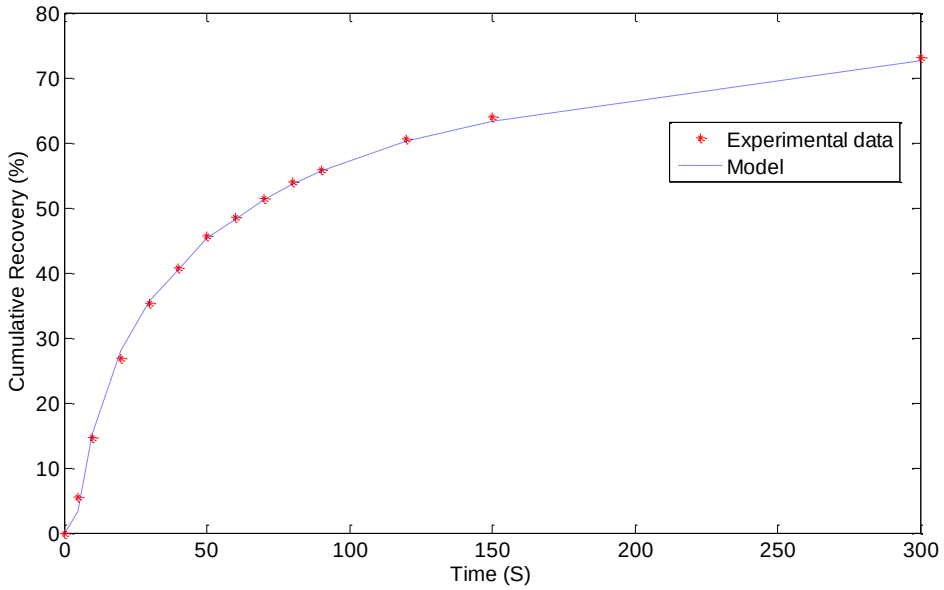

Figure 4-15: Comparing model predictions (based on the Kalman filter) with experimental data while parameter k_3 is being updated

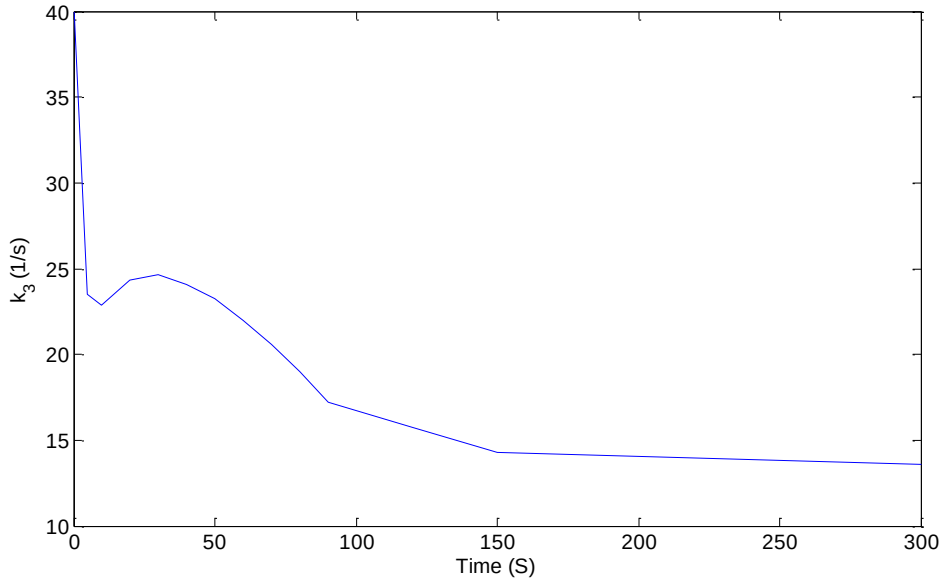

Figure 4-16: Estimate of parameter k_3 with time

The model parameters of run number 8 are given in table 4.3

Table 4-3: Model parameters

Parameter	Value	Remarks
Air flow rate (lit/min)	14	Constant
$V_p\ (m^3)$	$1.4\ x\ 10^{-3}$	Constant
$V_f\ (m^3)$	$0.26\ x\ 10^{-3}$	Constant
ϵ	0.55	Constant
$k_1\ (\frac{1}{S})$	Final value=65.58	Estimated and updated in simulation no. 1
$k_2\ (\frac{1}{S})$	Final value=32.73	Estimated and updated in simulation no. 2
$k_3\ (\frac{1}{S})$	Final value=104.52	Estimated and updated in simulation no. 3

The EKF simulation results for run number 8 are given in figures 4.17 to 4.22

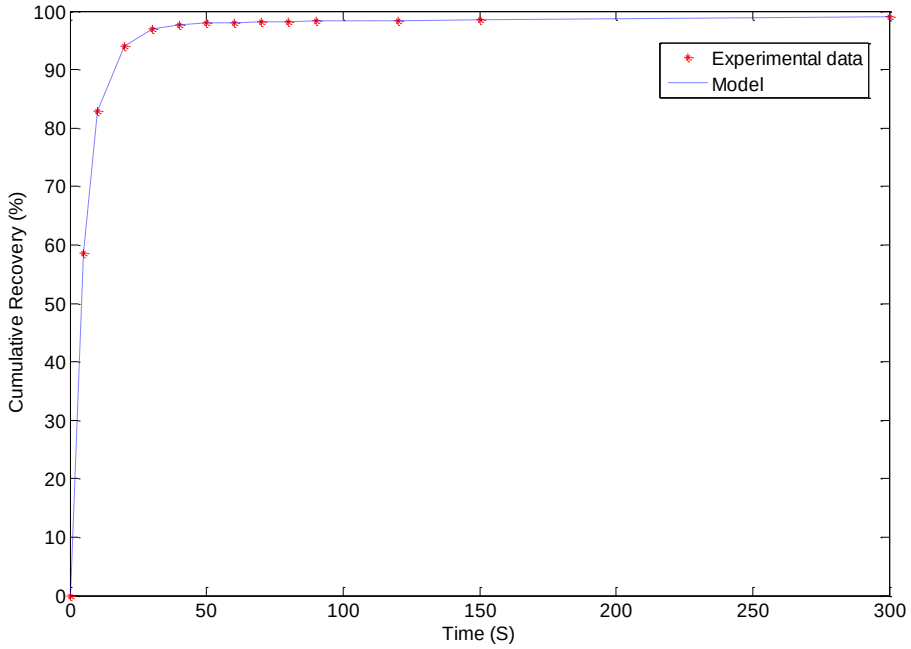

Figure 4-17: Comparing model predictions (based on the Kalman filter) with experimental data for run 8 while parameter k_1 is being updated

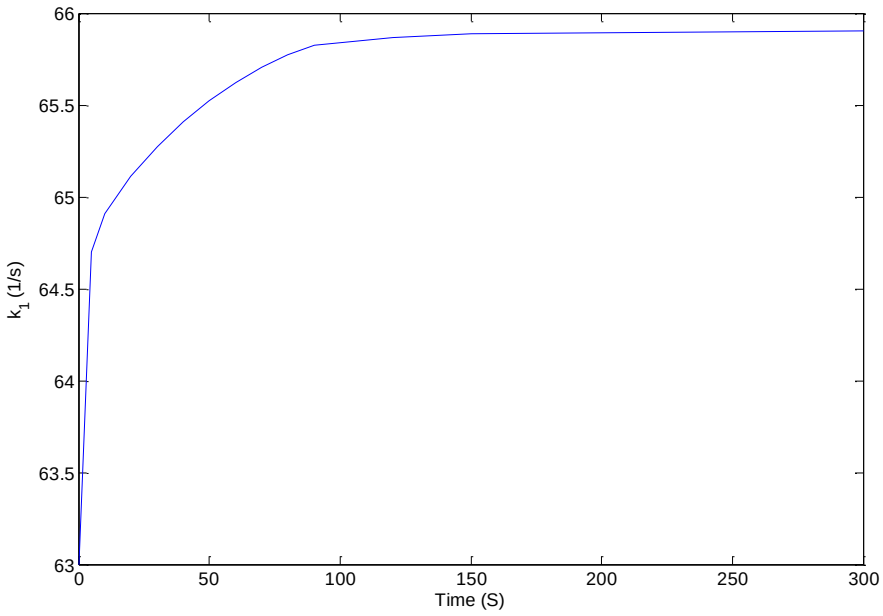

Figure 4-18: Estimate of parameter k_1 with time

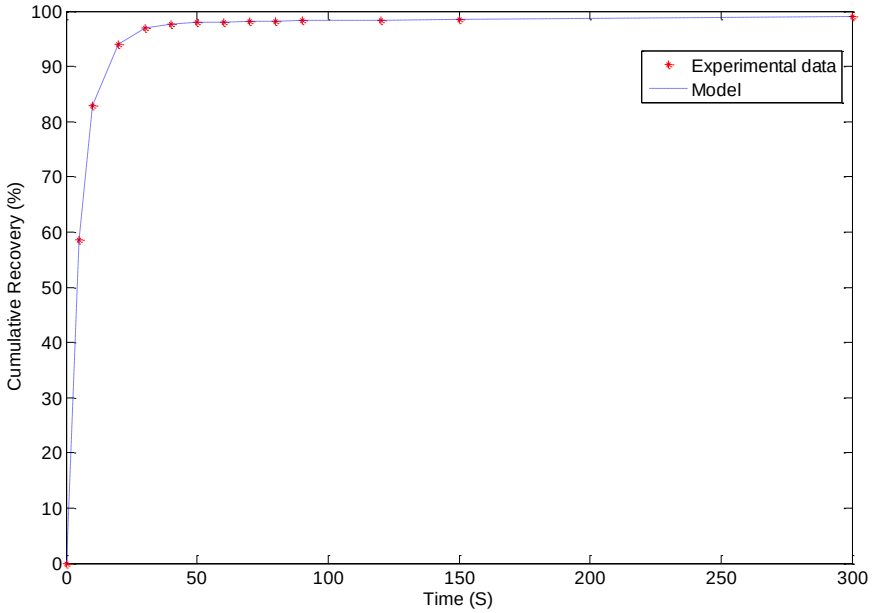

Figure 4-19: Comparing model predictions (based on the Kalman filter) with experimental data for run 8 while parameter k_2 is being updated

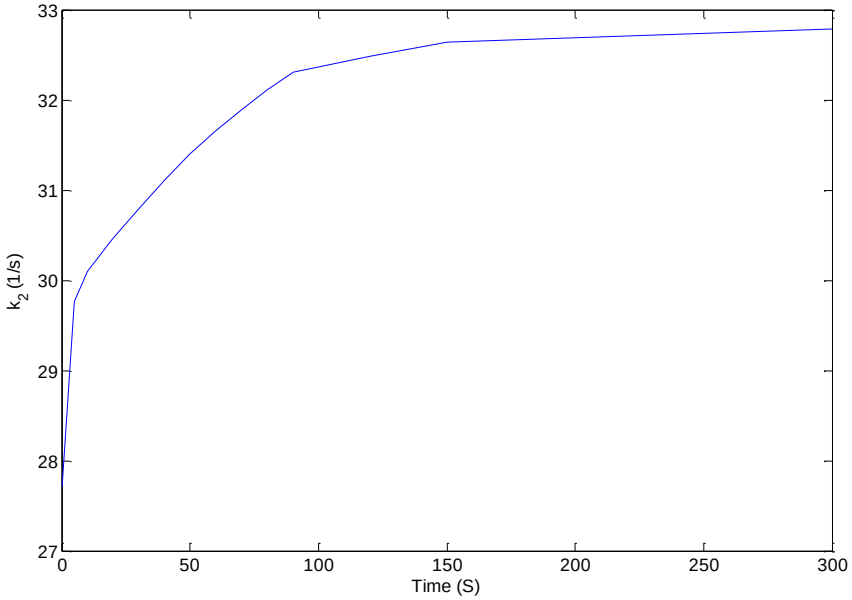

Figure 4-20: Estimate of parameter k_2 with time

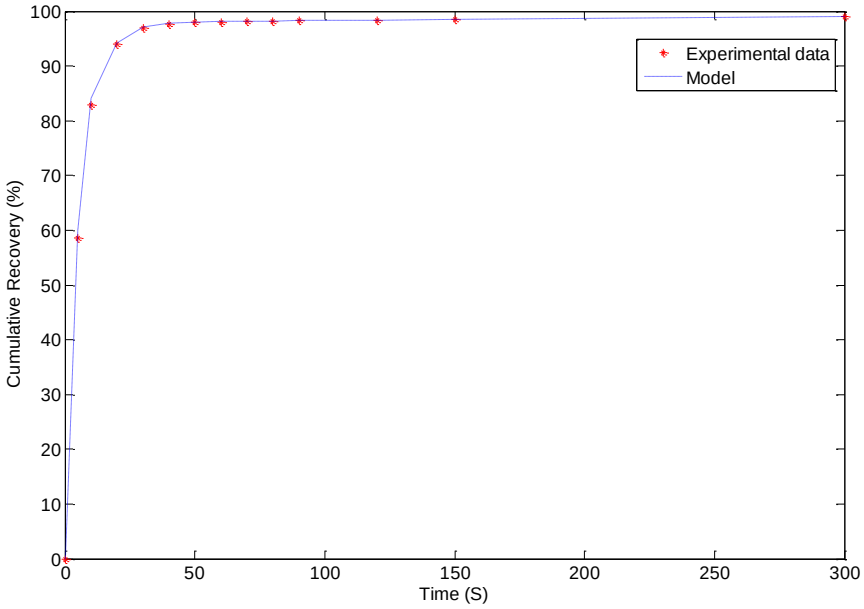

Figure 4-21: Comparing model predictions (based on the Kalman filter) with experimental data for run 8 while parameter k_3 is being updated

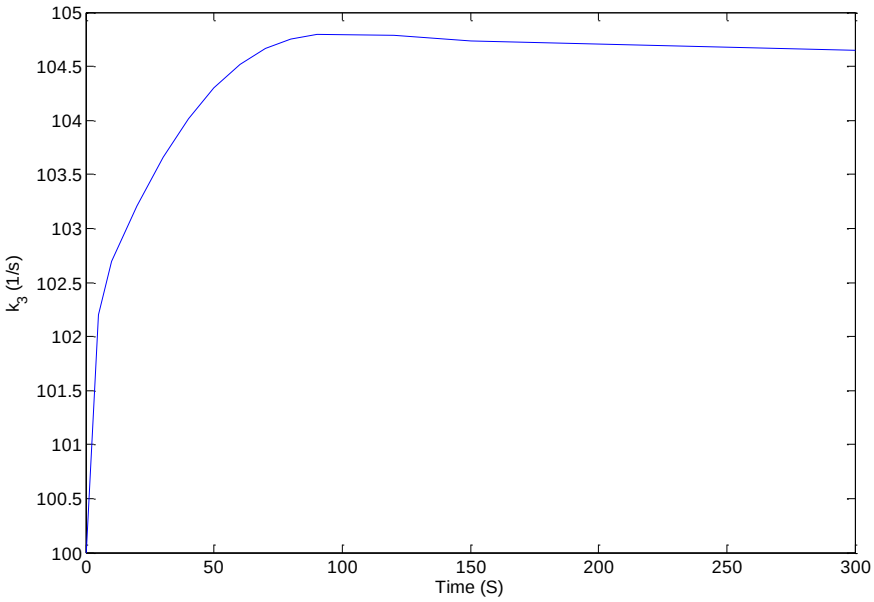

Figure 4-22: Estimate of parameter k_3 with time

4.6 Real-Time Updating of the Model Parameters Using Kalman Filter in the case of Disturbances

The ability of the extended Kalman filter estimator to track changes in operation and modifying parameter estimates is tested with two case studies. In the first case study, a disturbance is introduced in run number 1, whose operating conditions are given in table 4.4.

Table 4-4: Operating conditions for experimental run 1

Air flow-rate (lit/min)	Impeller speed (rpm)	Frother dosage (ml/lit slurry)	Collector dosage (mol/lit slurry)
14	1100	0.1	10^{-3}

At t=5 seconds, a step disturbance was applied to the flotation experiment, and the air flow-rate was changed from 14 lit/min to 8 lit/min. The EKF was used to track the recovery and estimate the states and the parameters of the system. Figure 4.23 shows that after the sudden decrease in air flow-rate, there is a significant decrease in cumulative recovery. This is because by lowering the air flow-rate, the flow-rate of the valuable mineral in the concentrate is decreased; therefore, the recovery decreases. With this disturbance in the system, the EKF could track the changes by updating the states and parameters as new measurements arrive and capture the dynamics of the system satisfactorily.

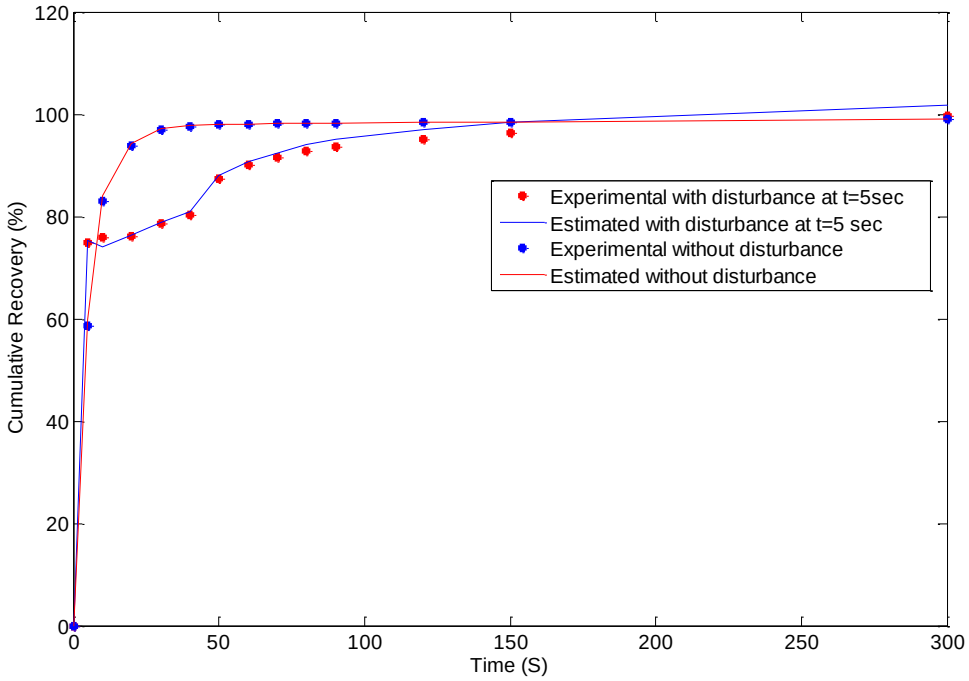

Figure 4-23: Comparison of cumulative recovery profiles for run 1 with a step disturbance applied in the air flow-rate at time t=5 s.

Figure 4.24 shows the EKF estimates for each of the parallel estimators for the three parameters of the system, ($k_1, k_2\ and\ k_3$), for run 1 with and without the disturbance. When the disturbance was applied to the system, the parameter k_1, which is related to the attachment, and parameter k_2, which is related to the detachment, did not change significantly in comparison to the condition when there was no disturbance. However, parameter k_3, which is related to the rate of transfer of particles to the concentrate from the froth phase, decreased because lowering the air flow rate resulted in a decrease in the amount of particles that are brought from the pulp phase to the froth phase; consequently, the rate of transfer of particles to the concentrate product would be decreased, too.

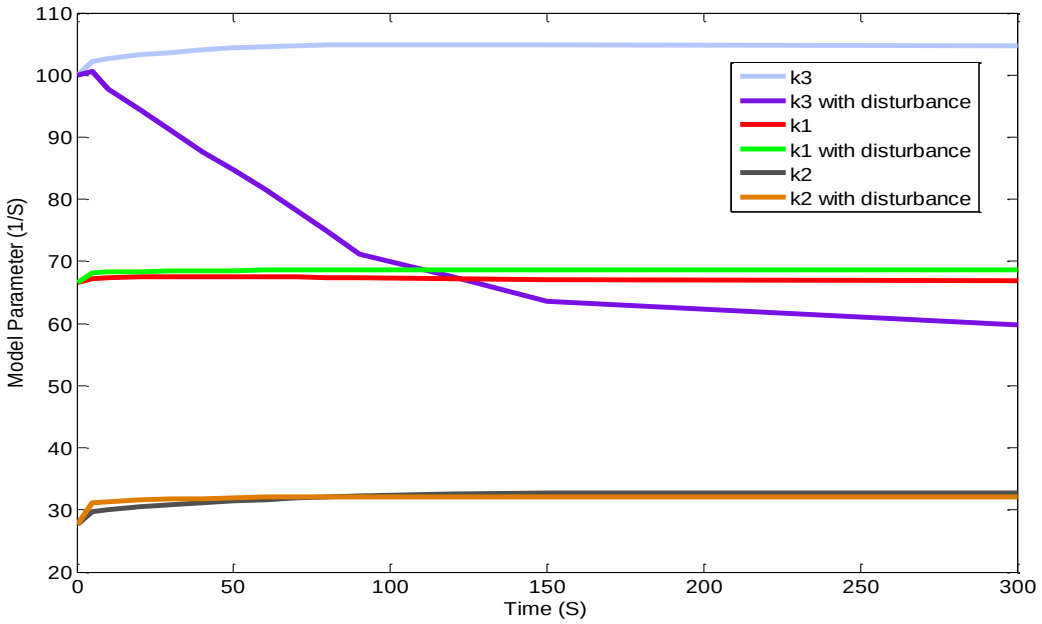

Figure 4-24: Comparison of parameter estimates with the disturbance of air flow rate

The second case study is based on run number 8, whose operating conditions are given in Table 4.5.

Table 4-5: Definitions for the parameters in the state space model

Air flow-rate (lit/min)	Impeller speed (rpm)	Frother dosage (ml/lit slurry)	Collector dosage (mol/lit slurry)
8	500	0.04	10^{-5}

At time t=5 seconds, a step disturbance was applied and the impeller speed was changed from $500\,rpm$ to $1100\,rpm$. The EKF was used to track the recovery and estimate the states and the parameters of the system. Figure 4.25 shows that with the increase in the impeller speed, there is an increase in the cumulative

recovery. Increasing the impeller speed in the pulp phase increases the bubble-particle interactions, leading to an increase in the probability of bubble-particle collision and therefore attachment, leading to an increase in the particles brought into the froth phase and consequently in the concentrate.

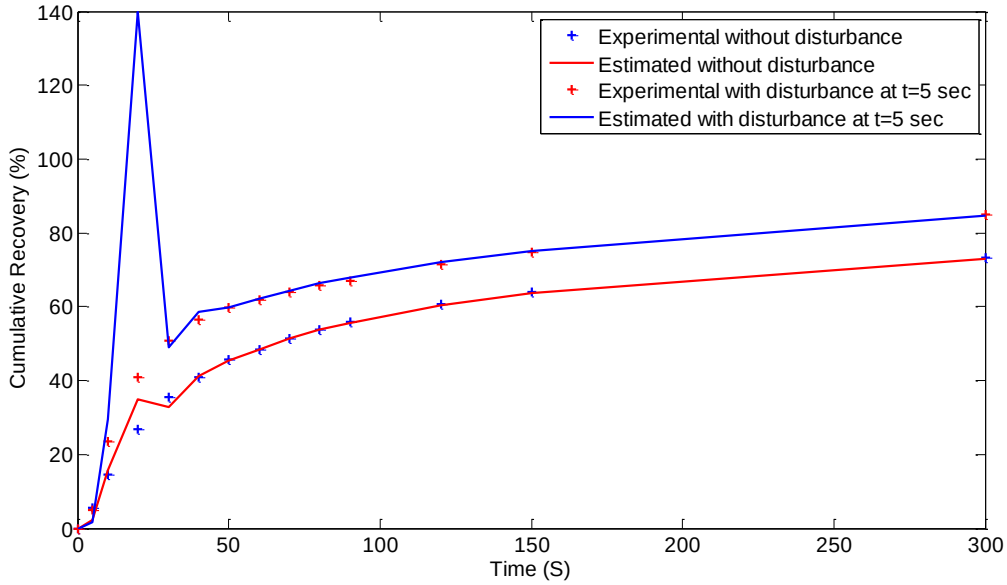

Figure 4-25: Comparison of cumulative recovery profiles with a step disturbance in impeller speed

Figure 4.26 shows the EKF estimates for each of the parallel estimators for the three parameters of the system, (k_1, k_2 and k_3), for run 1 with and without the disturbance. The estimates of parameters k_2 and k_3 did not change significantly\ but k_1, the rate of attachment, initially decreases due to the increased turbulence, and then increases due to the larger number of interactions between bubbles and particles. These results provide hope monitoring and fault diagnosis heuristics can be developed using parallel estimators for batch and continuous froth flotation processes.

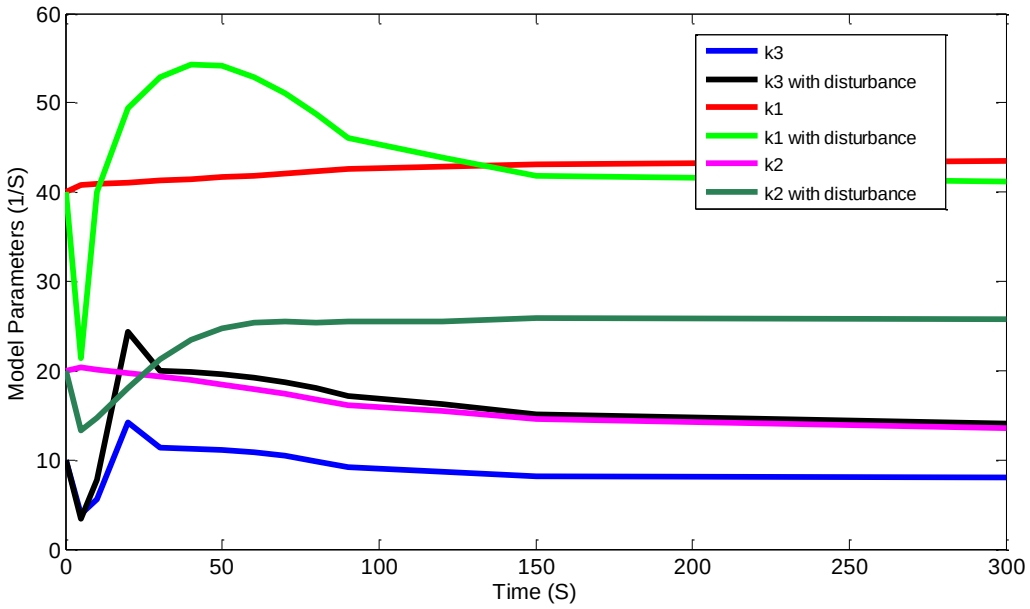

Figure 4-26: Comparison of parameter profiles with a step disturbance in impeller speed

Chapter 5

5 Conclusions & Future work

The objective of this study was developing a fundamental dynamic model for froth flotation process with parameters of the model being estimated and updated online with applicable techniques such as extended Kalman filtering. Most of the dynamic models that are proposed by previous researchers are empirical and a comprehensive fundamental model which could describe the whole flotation process by considering all phenomena happening in the different phases is not readily available. By using an online measurement, the parameters of the model were updated in real time and could provide insight into the physical processes governing the performance of the flotation system.

In the present study, various fundamental process models of different levels of complexity were investigated. The aim of considering different levels of complexity was to obtain the ability to describe transfer of the minerals between the phases, starting with mass action kinetics and going on to include more fundamental descriptions of attachment, detachment and transport. In the next step, a fundamental flotation framework based on population balances, hydraulic forces, mass transfer and kinetic equations for attachment and detachment and entrainment/drainage between the defined three states (phases) flotation cell was developed.

In order to validate the proposed model, a series of flotation experiments (eight runs) were performed under different operating conditions based on fractional

factorial design in a JK Tech batch flotation cell and the recovery of the system was calculated for each experiment. For every experimental run, the model was fitted to the experimental data and the parameters of the model were estimated offline.

The last and the main step of this research was focused on state estimation using extended Kalman filtering and updating the states and parameters of the system in real-time. The image processing setup, Visio-Froth, was placed at the top the flotation cell and the dynamic information for every run was captured. By using the online measurements from the Visio-Froth and applying the Kalman filtering technique in the model, the states and parameters of the model were estimated and updated online. For every run, the states and the parameters were updated in real-time and the output of the model which was predicting the recovery was calculated. The predicted recovery was compared to the experimental data for all of the runs. Furthermore, the ability of the Kalman filter estimator for tracking changes in operation and modifying the parameters estimations was tested with two disturbance case studies. The first disturbance at the t=5 was applied to the flotation experiment and the air flow-rate was changed from $14\ lit/min$ to $8\ lit/min$ and in the second disturbance, the impeller speed was changed from $500\ rpm$ to $1100\ rpm$. For both two disturbances, the EKF simulations, for predicting the final recovery, the states and the parameters of the system, were performed in order to predict the dynamic of the system. The results proved the ability of Kalman filtering in tracking changes and also by using the current approach, it was proved, even without knowing what type of disturbances

happening in the system, we are going to able to track changes in the system and determine the type of the disturbance.

In the next phase of the project, the continuous flotation column which is lately replaced by the current batch flotation cell, figure 5.1, will be used for further experiments. The proposed model should be also modified for this continuous system.

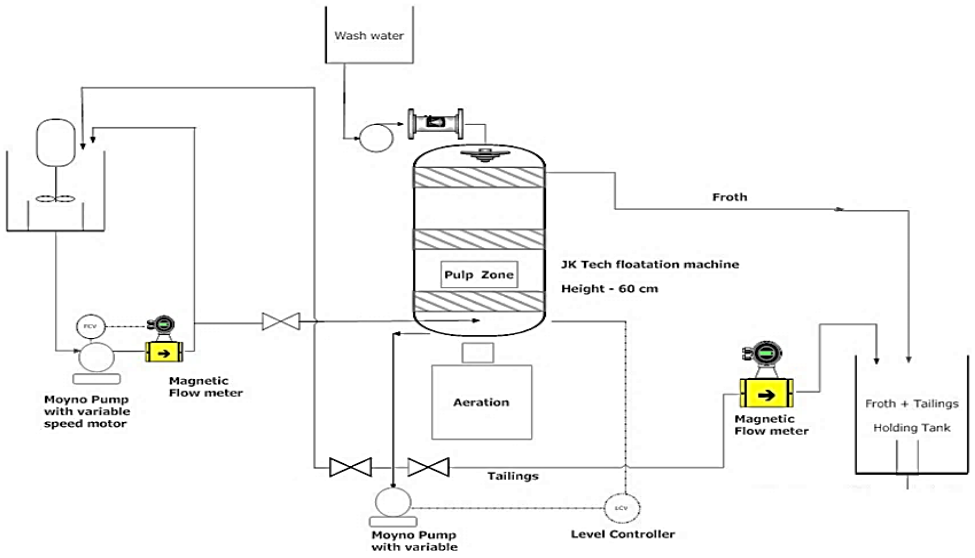

Figure 5-1: The continuous flotation column

The main issue in the aspect of modelling the flotation process is the rate of attachment and detachment in the pulp zone. Due to the complex nature of these two phenomena, most of the models that are proposed in the literature for calculating these two rates are empirical. Therefore, for future studies, further investigations for finding fundamental relationships between these rates and other physical characteristics of the flotation system is recommended. Furthermore, analyzing flotation column models, based on system identification methods,

which could perfectly describe the relationship between controlled variables and manipulated variables in the current continuous flotation setup, could be very helpful.

6 References

Ahmed N, Jameson G. Flotation Kinetics. 1989;5(1-4):77-99.

Amand FJS. Hydrodynamics of deinking flotation. Int J Miner Process 1999 4;56(1–4):277-316.

Bascur OA. An interactive dynamic flotation model framework. Proceedings of the XXI International Mineral Processing Congress; 2000 July 23-27; Rome, Italy; p. C8a-21-C8a-31

Batchelor GK. The theory of homogeneous turbulence.: Cambridge University Press; 1953.

Bikerman JJ. Foams. : Springer-Verlag New York; 1973.

Bloom F, Heindel TJ. Mathematical modelling of the flotation deinking process. Math Comput Model 1997 3;25(5):13-58.

Bloom F, Heindel TJ. Modeling flotation separation in a semi-batch process. Chemical Engineering Science 2003 1;58(2):353-365.

Bloom F, Heindel TJ. On the structure of collision and detachment frequencies in flotation models. Chemical Engineering Science 2002 7;57(13):2467-2473.

Bloom F, Heindel TJ. A Theoretical Model of Flotation Deinking Efficiency. J Colloid Interface Sci 1997 6/1;190(1):182-197.

Bushell C. Kinetics of flotation. Trans.AIME 1962;223:266-278.

Crawford R, Ralston J. The influence of particle size and contact angle in mineral flotation. Int J Miner Process 1988 5;23(1–2):1-24.

Crozier RD. Flotation. Theory, Reagents and Ore Testing. Pergamon Press plc(UK), 1992, 1992:356.

Cruz EB. A comprehensive dynamic model of the column flotation unit operation. PhD Thesis, Virginia Tech.; 1997.

Dobby GS, Finch JA. A model of particle sliding time for flotation size bubbles. J Colloid Interface Sci 1986 2;109(2):493-498.

Engelbrecht J, Woodburn E. The effects of froth height, aeration rate and gas precipitation on flotation. JS Afr.Inst.Min.Metall 1975;76(3):125-132.

Feteris SM, Frew JA, Jowett A. Modelling the effect of froth depth in flotation. Int J Miner Process 1987 6;20(1–2):121-135.

Finch JA, Dobby GS. Column flotation. : Pergamon Oxford; 1990.

Fuerstenau MC, Jameson GJ, Yoon RH. Froth flotation: a century of innovation. : SME; 2007.

Gorain BK, Napier-Munn TJ, Franzidis J-, Manlapig EV. Studies on impeller type, impeller speed and air flow rate in an industrial scale flotation cell. Part 5:

validation of k-Sb relationship and effect of froth depth. Minerals Eng 1998 7;11(7):615-626.

Hanumanth GS, Williams DJA. A three-phase model of froth flotation. Int J Miner Process 1992 5;34(4):261-273.

Heindel TJ. Fundamentals of flotation deinking. Tappi J 1999;82(3):115-124.

Heindel TJ, Bloom F. Exact and Approximate Expressions for Bubble–Particle Collision. J Colloid Interface Sci 1999 5/1;213(1):101-111.

Jameson G, Nam S, Young MM. Physical factors affecting recovery rates in flotation. Miner.Sci.Eng 1977;9(3):103-118.

Laplante AR, Toguri JM, Smith HW. The effect of air flow rate on the kinetics of flotation. Part 1: The transfer of material from the slurry to the froth. Int J Miner Process 1983 10;11(3):203-219.

Laskowski J. Particle bubble attachment in flotation. Mineral Science Eng 1974;6(4):223.

Leonard RA, Lemlich R. A study of interstitial liquid flow in foam. Part I. Theoretical model and application to foam fractionation. AICHE J 1965;11(1):18-25.

Luttrell GH, Yoon RH. A flotation column simulator based on hydrodynamic principles. Int J Miner Process 1991 11;33(1–4):355-368.

Mao L, Yoon R. Predicting flotation rates using a rate equation derived from first principles. Int J Miner Process 1997 10;51(1–4):171-181.

Mathe ZT, Harris MC, O'Connor CT. A review of methods to model the froth phase in non-steady state flotation systems. Minerals Eng 2000 2;13(2):127-140.

McFadzean B, Mhlanga SS, O'Connor CT. The effect of thiol collector mixtures on the flotation of pyrite and galena. Minerals Eng 2013 9;50–51(0):121-129.

Moys M. Mass transport in flotation froths. Mineral Procesing and Extractive Metallurgy Review 1989;5(1-4):203-228.

Neethling SJ, Lee HT, Cilliers JJ. Simple relationships for predicting the recovery of liquid from flowing foams and froths. Minerals Eng 2003 11;16(11):1123-1130.

Nguyen AV, Ralston J, Schulze HJ. On modelling of bubble–particle attachment probability in flotation. Int J Miner Process 1998 5;53(4):225-249.

Ogunnaike BA. Random Phenomena: Fundamentals of Probability and Statistics for Engineers. : CRC Press Inc; 2011.

Sawyerr F, Deglon D, O'Connor C. Prediction of bubble size distribution in mechanical flotation cells. Journal of the South African Institute of Mining and Metallurgy(South Africa) 1998;98(4):179-185.

Schulze HJ, Hecker M. Physico-chemical elementary processes in flotation: an analysis from the point of view of colloid science including process engineering considerations. : Elsevier Amsterdam; 1984.

Schulze H. The fundamentals of flotation deinking in comparison to mineral flotation. 1991.

Schulze HJ. Probability of particle attachment on gas bubbles by sliding. Adv Colloid Interface Sci 1992 5/30;40(0):283-305.

Sutherland K. Physical Chemistry of Floation. XI. Kinetics of the Flotation Process. 1948;52(2):394-425.

Tuteja RK, Spottiswood DJ, Misra VN. Mathematical models of the column flotation process a review. Minerals Eng 1994 12;7(12):1459-1472.

Ventura-Medina E, Cilliers JJ. A model to describe flotation performance based on physics of foams and froth image analysis. Int J Miner Process 2002 11;67(1–4):79-99.

Vera MA, Franzidis JP, Manlapig EV. Simultaneous determination of collection zone rate constant and froth zone recovery in a mechanical flotation environment. Minerals Eng 1999 10;12(10):1163-1176.

Vera MA, Mathe ZT, Franzidis J-, Harris MC, Manlapig EV, O'Connor CT. The modelling of froth zone recovery in batch and continuously operated laboratory flotation cells. Int J Miner Process 2002 3;64(2–3):135-151.

Verbist G, Weaire D, Kraynik AM. The Foam Drainage Equation. 1996;8(17):3715-3731.

Weaire D, Hutzler S. The Physics of Foams. illustrated, reprint ed. Great Clarendon Street, Oxford OX2 6DP: Oxford University Press; 1999.

Wehner JF, Wilhelm RH. Boundary conditions of flow reactor. Chemical Engineering Science 1956 11;6(2):89-93.

Welch G, Bishop G. An introduction to the Kalman filter 1995.

Woodburn E. Mathematical modelling of flotation processes. Miner.Sci.Eng 1970;2(2):3-17.

Yoon R, Luttrell G. The Effect of Bubble size on Fine Particle Flotation. 1989;5(1-4):101-122.

Yoon R, Mao L. Application of Extended DLVO Theory, IV: Derivation of Flotation Rate Equation from First Principles. J Colloid Interface Sci 1996 8/10;181(2):613-626.